Supplementary Information

Therapeutic Implications of Synonymous Gene Recoding: Insights into mechanisms controlling protein biogenesis and activity

Brian C. Lin[1†], Katarzyna I. Jankowska[1†], Upendra Katneni[1†], Randilu Amarasinghe[1], Nigam Padhiar[1], Nobuko Hamasaki-Katagiri[1], Wells W. Wu[2], Zhu Haojie[3], Hideki Taguchi[3], Arnab Ghosh[4#], David D. Holcomb[1], Je-Nie Phue[2], Sarah E. Fumagalli[1], Darón I. Freedberg[5], Ofer Kimchi[6], Rong-Fong Shen[2], Anton A. Komar[4], Zuben E Sauna[1], and Chava Kimchi-Sarfaty[1*]

[1] Division of Hemostasis, Office of Therapeutic Products, Center for Biologics Evaluation & Research, US FDA, Silver Spring, MD, 20993, USA
[2] Facility for Biotechnology Resources, Center for Biologics Evaluation & Research, US FDA, Silver Spring, MD, 20993, USA
[3] Cell Biology Center, Institute of Innovative Research, Tokyo Institute of Technology, Yokohama, 226-8503 Japan
[4] Center for Gene Regulation in Health and Disease and the Department of Biological, Geological and Environmental Sciences, Cleveland State University, Cleveland, Oh, 4415, USA
[5] Laboratory of Bacterial Polysaccharides, Division of Bacterial, Parasitic, and Allergenic Products, Center for Biologics Evaluation & Research, US FDA, Silver Spring, MD, 20993, USA
[6] Center for the Physics of Biological Function, Princeton University, Princeton, NJ, 08544, USA

[†] These authors contributed equally: Brian C. Lin, Katarzyna I. Jankowska, Upendra Katneni
[#] Presently at Integral Molecular, Philadelphia, PA, USA
* Corresponding author: Chava.Kimchi-Sarfaty@fda.hhs.gov

Materials and Methods

Design of codon and codon-pair optimized ADAMTS13 sequences

ADAMTS13 was codon optimized with Genscript's algorithm (GenSmart; https://www.genscript.com/gensmart-free-gene-codon-optimization.html). For the codon-pair optimized sequence, the following algorithm was designed to determine the optimal sequence:

Given an amino acid sequence $A_1, A_2, \ldots, A_n$, we aimed to find the codon-pair optimized DNA sequence, i.e. the codon sequence $C_1, C_2, \ldots, C_n$ that maximizes the codon-pair probability $P_{\text{pair}}(C_1, C_2, \ldots, C_n)$ subject to the constraint that codon C_i codes for amino acid A_i. The codon pair probability is defined as

$$P_{\mathbf{pair}}(C_1, C_2, \dots, C_n) = P(C_1)\prod_{i=1}^{n-1} P(C_{i+1}|C_i) \qquad (1)$$

where $P(C_{i+1}|C_i)$ is the probability of codon C_{i+1} given that it is preceded by codon C_i. The $P(C_1)$ term is determined by the first codon always being ATG.

To maximize $P_{\mathbf{pair}}(C_1, C_2, \dots, C_n)$, we first calculated the values for all codon pair probabilities $P(C_{i+1}|C_i)$. For this, we started from the genome of the desired organism (*homo sapiens* in this study) and counted the number of times each codon pair appears. We denoted the resulting 64×64 table of codon pair counts by N_{C_i,C_j}. For example, $N_{ATG,CAA}$ is the number of times an ATG codon is followed by a CAA codon. To correct for finite sampling, we added one to all counts.

We next changed the table of counts to one of probabilities. Specifically, we aimed to find the table $P(C_j|C_i)$: the probability of codon C_j appearing given that codon C_i preceded it. This is defined by

$$P(C_j|C_i) = \frac{N_{C_i,C_j}}{\sum_{C'} N_{C_i,C'}}.$$

We found it useful to consider the negative log probabilities $W(C_j|C_i) = -\log\left(P(C_j|C_i)\right)$, since the codon sequence that minimizes the sum of the negative log-probabilities must maximize the product of the probabilities in Eq. (1).

Then, we proceeded by defining a graph whose nodes are the possible codons that satisfy the amino acid sequence constraint. Edges are between codons that can follow one another. Each amino acid A_i corresponds to a set of nodes C_i, each of which is connected to all nodes corresponding to the previous amino acid, C_{i-1}, and to all nodes corresponding to the next amino acid, C_{i+1}. Edge weights are given by $W(C_{i+1}|C_i)$. We add an "end" node to which the stop codons are connected, with edge weight zero.

We then found the codon sequence that maximizes Eq. (1) by determining the shortest path through the graph, starting from the first node (ATG) and ending with the "end" node. We used Dijkstra's algorithm to solve this problem.

In silico analyses

For calculations involving computation of nucleotide or codon differences, CAI/CPAI, RSCU/RSCPU, %MinMax, CpG counts, and GC%, custom Python scripts were designed which relied on prior literature and publicly available analysis libraries (Alexaki et al. 2019; Kames et al. 2020). NUPACK software was used for secondary structure predictions (Zadeh et al. 2011) . For calculations involving translation rate, data from (Kim et al. 2015) was combined with custom Python code. For glycosylation analysis, initial processing was performed with Byonic/Byologic software suite, which generated normalized abundances for each glycan at specific ADAMTS13 positions. Visualizations of outputs were generated by custom python code.

For differential expression analysis, a custom pipeline was used to generate gene counts, as follows: 1) Trimmomatic software was used for read trimming (Bolger et al. 2014), 2) the STAR RNA-seq aligner was used to map reads to ribosomal RNA (to exclude these reads from subsequent analysis) (Dobin et al. 2013) 3) whole genome mapping was then performed with unmapped reads from step 2 to the GRCh38 genome using the same aligner 4) read counts were quantified with FeatureCounts software (Liao et al. 2013). After gene counts were generated, differential expression analysis was performed in R using a custom script that relied on a number of libraries (key among which are DESeq2 (Love et al. 2014), edgeR (Robinson et al. 2009), and clusterProfiler (Yu et al. 2012)).

Generation of ADAMTS13 WT, CO, and CPO vectors and cell lines

Cloning of variant *ADAMTS13* into pcDN5/FRT/V5-His Topo vector (ThermoFisher Scientific, Waltham, MA, USA) was performed by GenScript USA Inc. (Piscataway, NJ, USA). These vectors were used in transient transfection experiments and establishment of Flp-In stable expression cell lines. HEK293T cells ($1x10^6$ cells/well), seeded on 6-well plates and grown for 24h, were transiently transfected with Flp-in ADAMTS13 vectors (GenScript) using

Lipofectamine 3000 (Invitrogen) according to manufacturer protocol. Flp-In cell lines were generated as described previously (Jankowska et al. 2022).

HEK293T (ATCC) cell lines (empty and Flp-in) were maintained in Dulbecco's Modified Essential Medium (DMEM) with 10% fetal bovine serum (FBS), 100 U/mL penicillin, and 100 mg/mL streptomycin (Pen-Strep).

ADAMTS13 Protein purification

ADAMTS13 variants expressed from Flp-In stable expression cell lines were expressed in 4L bioreactors. Briefly, a BioFlo 320 control station (Eppendorf, Germany) was used together with a BioBLU 5p single-use packed-bed vessel with macrosparger (Eppendorf, Germany) for cell expansion and protein expression. Temperature, agitation, pH, and dissolved oxygen (DO) were controlled throughout the run. We cultivated Flp-In stable cells that expressed ADAMTS13 variants at 37°C and 80 rpm. Dissolved oxygen (DO) was measured using an optical DO sensor (Mettler Toledo®, Switzerland). DO was controlled at 50 % by automatic gassing at a flow of 0.006 – 0.05 SLPM in the 3-Gas Auto mode (air, oxygen, and CO_2) by sparger and 0.1 SLPM air supplied by overlay. The BioBLU 5p Single-Use Vessel was equipped with an optical pH sensor (PreSens, Germany) and the pH was controlled at 7.0-7.1 with CO_2. The BioBLU 5p single-use packed-bed vessel was inoculated with 8 x 108 cells to a working volume of 3.75 L of Dulbecco's Modified Eagle Medium including GlutaMAX™, pyruvate, PenStrep, and Poloxamer 188 (Gibco, Grand Island, NY, USA). Three days after inoculation, or when glucose concentration dropped to below 1 g/l, the medium was removed from the bioreactor and 3.75 L of fresh medium was added. After four replacements of the medium for cell expansion, the medium was replaced with Opti-MEM I Reduced Serum medium (Gibco, Grand Island, NY, USA) for protein expression. The cells were incubated in this medium for 48 hours, and then the medium was collected and replaced with a fresh batch of protein expression medium at every two-day interval repeated four times. The collected media were purified by using anion exchange chromatography followed by anti-V5-tag affinity chromatography as described previously (Jankowska et al. 2022).

DNA and RNA isolation and measurement through RT-qPCR

To determine the level of ADAMTS13 gene expression of WT, CO and CPO variants stable expressed in Flp-In HEK293 cells were cultured for 48h on 6-well plates. Total RNA from cell pellets was isolated using RNeasy Plus Mini Kit (Qiagen) according to the manufacturer's instructions. To detect the relative levels of ADAMTS13 mRNA in each variant, Reverse Transcription Quantitative PCR (RT-qPCR) was performed. For ADAMTS13, the cDNA was generated by reverse transcription (High-Capacity cDNA Reverse Transcription Kits Applied Biosystems). PCR products were quantitatively synthesized from cDNA samples with a reagent solution and RT-qPCR gene expression study (TaqMan Gene Expression Master Mix and TaqMan Gene Expression Assays specific to V5-tag (Custom designed primers from ThermoFisher) and 18S (Hs99999901, ThermoFisher) as an endogenous control. The reaction conditions followed the manufacturer's instructions. The fold change for each target gene or target miRNA relative to the control group was calculated using the ΔΔCt method.

Protein expression through SDS-PAGE and immunoblotting

Determination of ADAMTS13 levels from cells, media or purified ADAMTS13 proteins by SDS-PAGE and Western Blotting were described previously (Jankowska et al. 2022). For purified protein assays, amount of protein was measured using A280 measurement with NanoDrop Spectrophotometer (NanoDrop One C Microvolume UV Vis Spectrophotometer, ThermoScientific) and confirmation with SDS-PAGE and Coomassie staining (Coomassie Brilliant Blue R-250 Staining Solution #1610436, Bio-Rad). Immunoblots were imaged with the Odyssey DLx Imaging System (LICORbio) after being probed with IRDye 680 and 800CW secondary antibodies. Quantification of band intensities were determined using ImageJ.

ADAMTS13 FRETS-VWF73 activity assay

Activities of ADAMTS13 proteins was measured through fluorescent resonance energy transfer (FRET) assay with fluorescent FRETS-VWF73 substrate (Vivitide, Gardner, MA, USA) as described previously (Jankowska et al. 2022; Kokame et al. 2005). Briefly, rADAMTS13 media collected from cultures or purified rADAMTS13 proteins (2 ng/µl) were diluted in FRET assay buffer (5 mM Bis–Tris, 25 mM $CaCl_2$, 0.005%, Tween-20, pH 6.0) to the volume of 70µl

and incubated at 37 °C for 5 min. Then, 80 µl FRETS-VWF73 substrate diluted in FRETS-VWF73 assay buffer to the final concentration of 2 µM (unless specified differently) was added to each well. After combining, 60 total fluorescence readings were taken at 1-min intervals by a Victor X3 plate reader (PerkinElmer, Waltham, MA, USA). ADAMTS13 activity was determined as the slope (fluorescence/time, dF/dt [1/min]). Specific activity was determined as the activity (IU/mL) divided by the antigen levels (ng/mL), measured through WB. At least three sets of purified rADAMTS13 and media from culture collections were analyzed.

VWF Digestion by ADAMTS13 variants

The impact of conformational differences between ADAMTS13 variants on their potential ability to cleave full-length VWF was assessed by this assay. In this assay, the digestion of recombinant VWF by ADAMTS13 variants (WT, CO and CPO) was performed for 15 minutes at 37 ˚C under 2500 rpm vertexing conditions in a 30 µl reaction. Reaction buffer used in the digestion reaction is composed of 5mM CaCl2, 150mM NaCl and 20mM HEPES. Following the completion of incubation, the reaction was stopped by adding equal volume of 2X LDS Sample buffer (ThermoFisher, NP007) and heating reaction mix at 100 ˚C for 20 minutes. The digestion samples were analyzed following non-reducing SDS-PAGE and probing for VWF digestion bands using anti-VWF polyclonal antibody (Abcam, ab9378). No significant differences were observed between the digested VWF samples in this assay (Supplementary Fig. 4)

ADAMTS13 antibody inhibitory assay

Anti-ADAMTS13 monoclonal antibody, 3H9 (Feys et al. 2010), which was produced against human rADAMTS13 with its epitope mapped to metalloprotease domain and reported to inhibit baboon plasma ADAMTS13, was a kind gift from Dr. Karen Vanhoorelbeke (Kokame et al. 2005). rADAMTS13 samples (WT, CO, and CPO) at 133 ng/mL concentration were incubated with serial dilutions (0.003 – 10 nM) of 3H9 at 30 °C for 30 min. ADAMTS13 activity was then measured by chromogenic assay using FRETS-VWF73 substrate (Peptide Institute Inc., #3224-S). The Dose Response Curve R package was used to find the difference in loglikelihoods of the retained ADAMTS13 activity after inhibition (Ritz et al. 2016). The best fit regressions were determined for models that distinguished between treatment types and not. These models were then compared using the test. Estimated half-max (ED50) values were calculated using 3-

parameter dosage response curves stratified by treatment type. Significance was determined via the Bonferroni alpha adjustment (0.01/3). Assessment of conformational differences in recoded ADAMTS13 variants by this assay revealed no statistically significant differences (Supplementary Fig. 5).

Kinetics analysis with fitting with Michaelis-Menten kinetics

ADAMTS13 activities from transient and Flp-In stable integration systems were measured at constant concentration with purified ADAMTS13 proteins (2 ng/µl) or constant volume of extracellular media (20 µl) with different concentrations of FRETS-VWF73 (0.05-3.2 µM). The rate of these reactions (dF/dt) were plotted as functions of substrate concentration (dF/dt) vs concentrations of FRETS-VWF73. Curves were fitted to the Michaelis–Menten equation. Kinetic parameters (Km, Vmax) were calculated using PRISM V9 software (GraphPad Software, San Diego, CA, USA).

Binding Assays

VWF-ADAMTS13 association-dissociation kinetics were determined by biolayer interferometry (BLI) using an Octet RED96 (ForteBio). Recombinant GST-VWF73 (VWF73) substrate from Technozym ADAMTS13 activity ELISA kit (Technoclone) was captured by Octet GST biosensors (Sartorius)., with binding of ADAMTS13 variants performed in PBS, 2 mg/mL BSA, and 0.02% Tween 20 at various protein concentrations (1.6-0.05 µM) followed by dissociation in PBS buffer. Binding kinetics were monitored by Octet Data Acquisition 8.2.0.9. Dissociation constants from steady state affinities (response at equilibrium (Req, nm) vs ADAMTS13 concentration were determined from global kinetic analysis for a 1:1 binding model using Octet RED software (ForteBio Data Analysis, version 8.2).

Affinity kinetics analyses were performed in Prism through fitting of association and dissociation response signals vs time using nonlinear regression. Dissociation rate (k_{on}, min^{-1}.), association rate (k_{off}, $M^{-1}min^{-1}$), dissociation constant $K_D = k_{off}/k_{on}$ (M), and maximum binding at equilibrium (R_{max}, nm), were determined from affinity curves (response vs time) measured at various concentrations. Buffer-only reference was subtracted from all curves. Y-axis alignment and inert-step correction to the dissociation signal was performed prior to steady-state and time-

resolved analysis. Data from four different sets of purified ADAMTS13 were analyzed, combined, and presented as mean values.

In vitro translation

Transcription/translation coupled rabbit reticulocyte lysate system (TnT coupled RRL) (Promega) was used to translate ADAMTS13. Components for 10 µl translation system, including 5 µl 2xTnT rabbit reticulocyte lysate, 0.4 µl TnT reaction buffer, 0.2 µl TnT RNA polymerase, 2.8 µl amino acid (1 mM each), 0.2 µl Rnase inhibitor, 0.4 µl DNA template (500 ng/µl), and 1 µl protease inhibitor cocktail (EDTA free), were mixed well and incubated at 30 °C. Aliquots were withdrawn at 25, 32, 41, 50, 60, 90, 120, and 180 min. The samples before ultracentrifugation were denoted as [T], and post-centrifugation supernatant samples as [S] and detected by CBB staining and Western blotting using an anti-FLAG antibody. The kinetic data were fitted to obtain kinetic parameters as previously described *(Samelson et al. 2018)*.

Circular Dichroism (CD) Spectropolarimetry of purified ADAMTS13

CD analysis of ADAMTS13 was performed using a J-819 CD Spectrophotometer (Jasco). Concentrations were measured using NanoDrop Spectrophotometer (NanoDrop One C Microvolume UV Vis Spectrophotometer, ThermoScientific) and Coomassie staining (Coomassie Brilliant Blue R-250 Staining Solution #1610436, Bio-Rad). CD measurements were performed on 3 sets of purified ADAMTS13 variants. CD spectra was measured under unfolding/refolding protocols as described previously (Katneni et al. 2022). Secondary structure estimation was predicted with BestSel software (Micsonai et al. 2018).

Cycloheximide chase

Cycloheximide (CHX)-chase protein stability experiments were performed by adding CHX to cultures (100 µM final concentration) and incubating at 37 °C in 5% CO_2. Cultures were removed at appropriate time intervals (up to 6h), washed two times with 1x PBS and lysed using cell lysis buffer (Cell Lysis Buffer #9803, Cell Signaling Technology). Lysates were sonicated (Digital Heated Ultrasonic Cleaner, Branson CPX2800H), protein concentrations were

determined by BCA, and equal amounts of protein were used for SDS-PAGE and immunoblotting.

Post-Translational Modifications (PTMs)

PTMs of purified ADAMTS13 proteins were evaluated through peptide mapping via tryptic digestion as previously described (Peters et al. 2013). Glycosylation analysis of ADAMTS13 derived from Flp-In stable expression cell lines was performed as described previously (Jankowska et al. 2022) with minor modifications in data analysis. LC/MS/MS spectra were processed using Byonic software and automated quantitative analysis was performed using Byologic software (PMI‐Suite 5.3.5, Protein Metrics, Cupertino, CA, USA), which uses as input both MS1 raw data and Byonic search results. The data were analyzed according to (Zhu et al. 2019) and presented as the peak area of the extracted ion chromatograms (XICs) of a given glycopeptide that was automatically integrated and normalized against the total glycopeptides of ADAMTS13 variants identified in each MS run.

Byonic/Byologic search parameters were set according to the parameters employed: tryptic cleavage sites @K/R (fully specific), two mis‐cleavage allowed, 25 ppm mass tolerance, common modification of oxidation @M, fixed modification of carbamidomethylation @C, protein database of ATS13_HUMAN, and PEP 2D / Score / Delta Mod Score being ≤0.01, ≥100, ≥10, respectively.

For identifications of O‐fucosylation and C‐mannosylation, common modification of mannosylation @W was further added, and the glycan database consists of Fuc(1), Fuc(1)Hex(1), HexNAc(1)Hex(1)NeuAc(2), and HexNAc(2)Hex(2)NeuAc(2). For identifications of N‐linked glycosylation, the Byonic glycan database of "N‐glycan 182 human no multiple fucose.txt" was used.

It should be noted here that the PTM studies were performed twice for each variant. The first run was performed separately for each ADAMTS13 variant (non-quantitatively). These results were partially published previously (Hunt et al. 2019; Jankowska et al. 2022). From these studies, we learned that the same N-sites are glycosylated in the ADAMTS13 variants as in the

wild-type (WT). However, we observed different glycan profiles in each ADAMTS13 variant, which we had not expected. These findings prompted us to conduct a more quantitative analysis. Our quantitative evaluation, presented in the manuscript, has further confirmed the glycan differences in ADAMTS13. Due to slightly varying experimental design, we cannot treat them as replicates for statistical analysis; however, both experiments showed similar results for a majority of the most abundant glycans, which is strong supporting evidence of their presence in these samples (see **Supplementary Fig. 11**).

ER stress, proteolysis, and Immunoprecipitation

Intracellular lysates and extracellular media were separated using SDS-PAGE and immunoblotting. The following antibodies were used to probe for ER stress markers, including anti-BiP (115870-1-AP, ProteinTech), anti-eIF2α (#9722, Cell Signaling Technology), anti-phosphorylated-eIF2α (#9721, Cell Signaling Technology) and mouse anti-V5 antibody (ThermoFisher).

Immunoprecipitation Assays for ADAMTS13-BiP interactions were performed using affinity tag purification anti-V5 tag gel resin (MBL International) as described previously (Hunt et al. 2019). Immunoprecipitated lysates pull-downed with the V5-tag resin were separated with SDS-PAGE and immunoblotted. Blots were probed with mouse anti-V5 antibody (ThermoFisher) and anti-BiP (115870-1-AP, ProteinTech) antibodies.

Seahorse Respiration Assays

Seahorse XF24 V7 plates (Agilent Technologies) were used for performing Seahorse respiration assays under standard manufacturers' protocols. 60,000 cells/100 µl was determined to be an optimal seeding density for HEK293 cells. 4-5 replicates were plated in randomized positions into the XF24 wells, grown overnight in the Seahorse plate, and on the subsequent day, cells were washed with Seahorse assay media and equilibrated in media for 1h. Cell density, morphology, and health were monitored under a light microscope. At the same time, Seahorse cartridges were switched to XF calibrant solution and cassettes were loaded with oligomycin, FCCP and antimycin/rotenone at optimal titrated concentrations (oligomycin/antimycin

A/rotenone [1 μM]; FCCP [2 μm]). Seahorse assay was run on Seahorse XFe24 Analyzer (Agilent), through standard Mito Stress Test assay protocols.

MHC-associated Peptide Proteomics Assay

Study was performed by ProImmune, Oxford, UK as described previously (Jankowski et al. 2019). Peripheral blood mononuclear cells isolated from whole blood samples of a panel of 12 healthy donors who were selected to represent HLA class II alleles that are known to be highly expressed in the global population were used.

Dendritic T-cell proliferation assay

The study was performed by ProImmune, Oxford, UK. Peripheral blood mononuclear cells (PBMCs) and autologous T-cells isolated from peripheral blood samples of 31 healthy donors, which were selected to represent HLA class II alleles, known to be highly expressed in the global population, were used in the assay. Adherent PBMCs were cultured with appropriate growth factors to generate monocyte-derived dendritic cells. Dendritic cells were loaded with either test proteins (final concentration = 0.34 μM), control proteins (Tuberculin purified protein derivative and Keyhole Limpet Hemocyanin proteins at a final concentration of 5 μg/mL and 0.25 mg/mL, respectively) or left untreated. Antigen-loaded dendritic cells were co-cultured with a fixed ratio of autologous CFSE labelled T-cells for 7 days. Each reaction was set up in eight replicate wells. Following incubation, cells were stained with anti-CD4 antibody and analyzed by flow-cytometry for CFSE intensity. Responses to test proteins were reported as: i) percentage of antigenicity – measured using the frequency of donors exhibiting percentage stimulation above background (e.g., ≥ 0.5%) and ii) response index, which accounts for frequency and strength of response.

References

Alexaki, A., et al. (2019), 'Codon and Codon-Pair Usage Tables (CoCoPUTs): Facilitating Genetic Variation Analyses and Recombinant Gene Design', *J Mol Biol,* 431 (13), 2434-41.

Bolger, A. M., Lohse, M., and Usadel, B. (2014), 'Trimmomatic: a flexible trimmer for Illumina sequence data', *Bioinformatics,* 30 (15), 2114-20.

Dobin, A., et al. (2013), 'STAR: ultrafast universal RNA-seq aligner', *Bioinformatics,* 29 (1), 15-21.

Feys, H. B., et al. (2010), 'Thrombotic thrombocytopenic purpura directly linked with ADAMTS13 inhibition in the baboon (Papio ursinus)', *Blood,* 116 (12), 2005-10.

Hunt, R., et al. (2019), 'A Single Synonymous Variant (c.354G>A [p.P118P]) in ADAMTS13 Confers Enhanced Specific Activity', *Int J Mol Sci,* 20 (22).

Jankowska, Katarzyna I., et al. (2022), 'An Optimized Purification Design for Extracting Active ADAMTS13 from Conditioned Media', *Processes,* 10 (2), 322.

Jankowski, Wojciech, et al. (2019), 'Peptides identified on monocyte-derived dendritic cells: a marker for clinical immunogenicity to FVIII products', *Blood Advances,* 3 (9), 1429-40.

Kames, J., et al. (2020), 'TissueCoCoPUTs: Novel Human Tissue-Specific Codon and Codon-Pair Usage Tables Based on Differential Tissue Gene Expression', *J Mol Biol,* 432 (11), 3369-78.

Katneni, Upendra K, et al. (2022), 'Structural, functional, and immunogenicity implications of F9 gene recoding', *Blood Advances*.

Kim, Soo Jung, et al. (2015), 'Translational tuning optimizes nascent protein folding in cells', *Science,* 348 (6233), 444-48.

Kokame, Koichi, et al. (2005), 'FRETS-VWF73, a first fluorogenic substrate for ADAMTS13 assay', *British Journal of Haematology,* 129 (1), 93-100.

Liao, Yang, Smyth, Gordon K., and Shi, Wei (2013), 'featureCounts: an efficient general purpose program for assigning sequence reads to genomic features', *Bioinformatics,* 30 (7), 923-30.

Love, Michael I., Huber, Wolfgang, and Anders, Simon (2014), 'Moderated estimation of fold change and dispersion for RNA-seq data with DESeq2', *Genome Biology,* 15 (12), 550.

Micsonai, A., et al. (2018), 'BeStSel: a web server for accurate protein secondary structure prediction and fold recognition from the circular dichroism spectra', *Nucleic Acids Res,* 46 (W1), W315-w22.

Peters, R. T., et al. (2013), 'Biochemical and functional characterization of a recombinant monomeric factor VIII-Fc fusion protein', *J Thromb Haemost,* 11 (1), 132-41.

Ritz, Christian, et al. (2016), 'Dose-Response Analysis Using R', *PLOS ONE,* 10 (12), e0146021.

Robinson, Mark D., McCarthy, Davis J., and Smyth, Gordon K. (2009), 'edgeR: a Bioconductor package for differential expression analysis of digital gene expression data', *Bioinformatics,* 26 (1), 139-40.

Samelson, Avi J., et al. (2018), 'Kinetic and structural comparison of a protein's cotranslational folding and refolding pathways', *Science Advances,* 4 (5), eaas9098.

Yu, G., et al. (2012), 'clusterProfiler: an R package for comparing biological themes among gene clusters', *Omics,* 16 (5), 284-7.

Zadeh, J. N., et al. (2011), 'NUPACK: Analysis and design of nucleic acid systems', *J Comput Chem,* 32 (1), 170-3.

Zhu, Jianhui, et al. (2019), 'Differential Quantitative Determination of Site-Specific Intact N-Glycopeptides in Serum Haptoglobin between Hepatocellular Carcinoma and Cirrhosis Using LC-EThcD-MS/MS', *Journal of Proteome Research,* 18 (1), 359-71.

Supplementary Figures

A

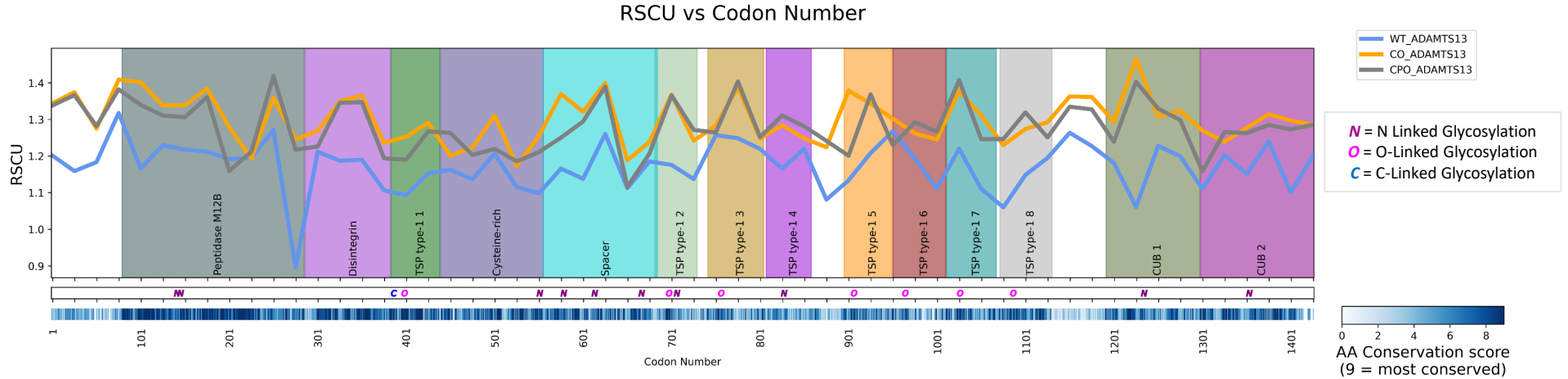
RSCU vs Codon Number
RSCU
Codon Number
Peptidase M12B
Disintegrin
TSP type-1 1
Cysteine-rich
Spacer
TSP type-1 2
TSP type-1 3
TSP type-1 4
TSP type-1 5
TSP type-1 6
TSP type-1 7
TSP type-1 8
CUB 1
CUB 2
WT_ADAMTS13
CO_ADAMTS13
CPO_ADAMTS13
N = N Linked Glycosylation
O = O-Linked Glycosylation
C = C-Linked Glycosylation
AA Conservation score
(9 = most conserved)

B

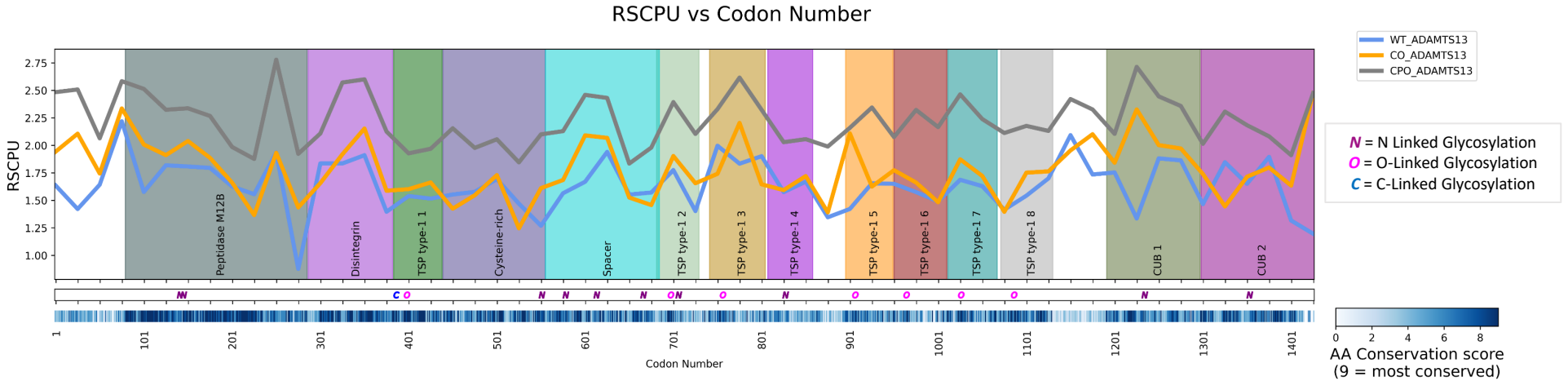
RSCPU vs Codon Number
RSCPU
Codon Number
Peptidase M12B
Disintegrin
TSP type-1 1
Cysteine-rich
Spacer
TSP type-1 2
TSP type-1 3
TSP type-1 4
TSP type-1 5
TSP type-1 6
TSP type-1 7
TSP type-1 8
CUB 1
CUB 2
WT_ADAMTS13
CO_ADAMTS13
CPO_ADAMTS13
N = N Linked Glycosylation
O = O-Linked Glycosylation
C = C-Linked Glycosylation
AA Conservation score
(9 = most conserved)

C

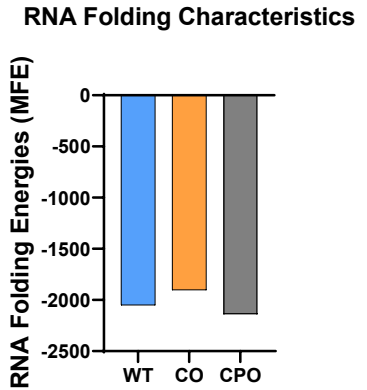
RNA Folding Characteristics
RNA Folding Energies (MFE)
WT
CO
CPO

D

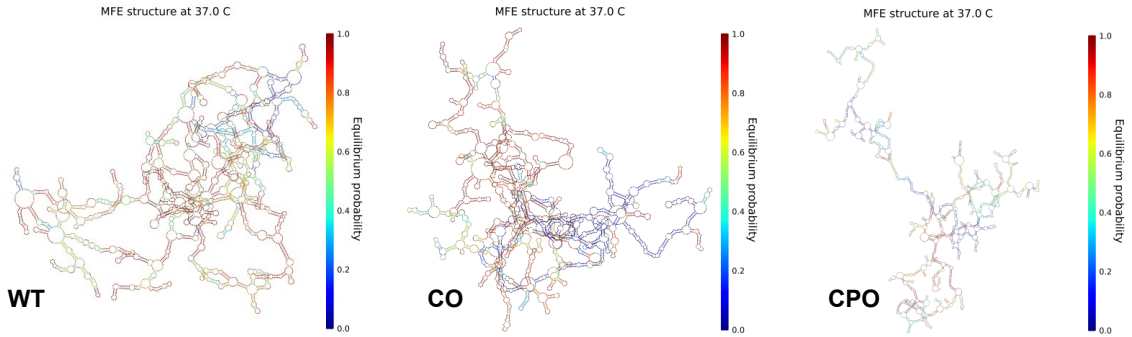
MFE structure at 37.0 C
Equilibrium probability
WT
CO
CPO

E

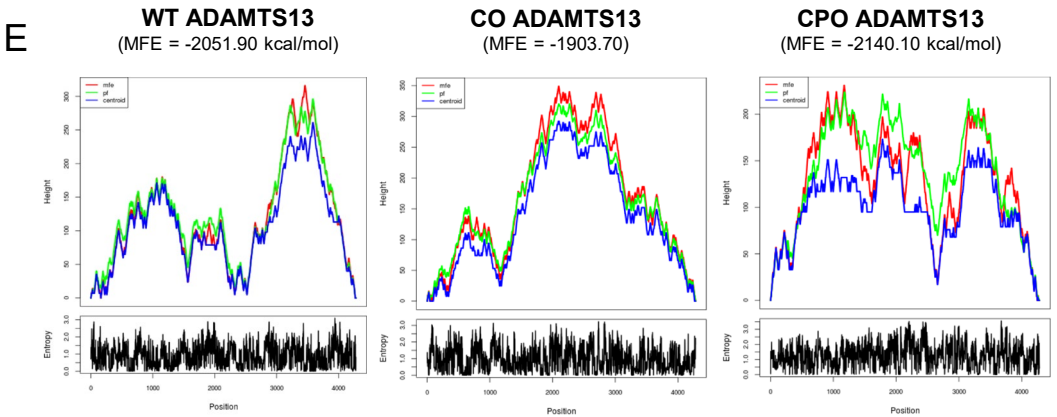
WT ADAMTS13
(MFE = -2051.90 kcal/mol)
CO ADAMTS13
(MFE = -1903.70)
CPO ADAMTS13
(MFE = -2140.10 kcal/mol)
Height
Entropy
Position

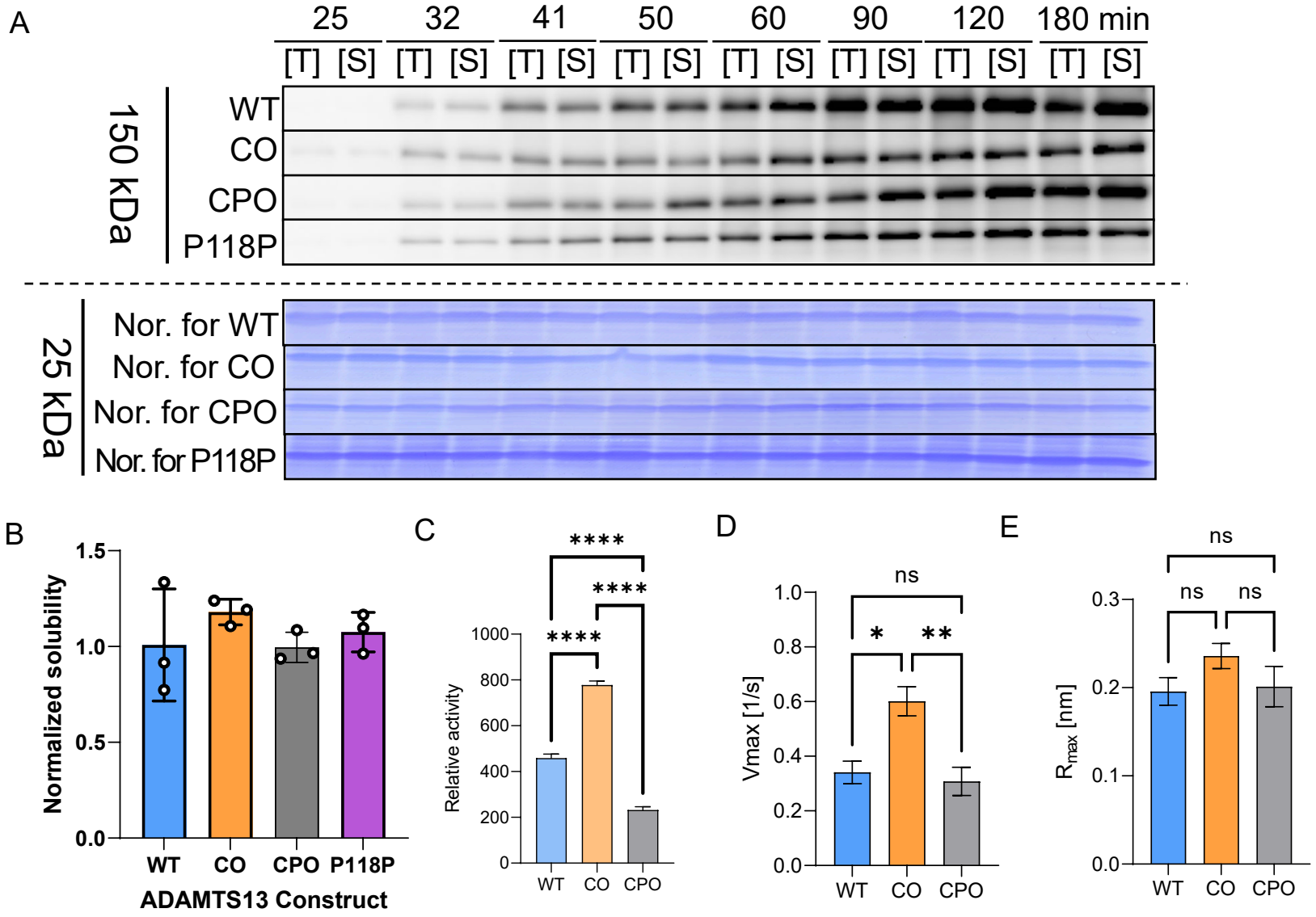

Supplementary Fig. 2: Kinetic analysis of ADAMTS13 variants. (A) Representative blotting of ADAMTS13 by RRL translation at multiple time points (upper panel) and the CBB staining for normalization (lower panel) used to calculate product concentration in Fig. 1C. **(B)** The solubility of ADAMTS13 from RRL assay at 180 min were similar between *ADAMTS13* variants (Statistically non-significant). **(C)** Activity of extracellular media, as measured by FRETS-VWF73 activity assay (dF/dt, [1/min]), used to calculate apparent specific activity in Fig. 1G, **(D)** FRETS activity assay with increasing VWF concentration and data was fitted with Michaelis Menten equation to derive kinetic values for Vmax, again showing significant changes in CO *ADAMTS13*. **(E)**, Maximum binding at equilibrium (R_{max}) determined from steady state analysis (nonlinear fitting of response at equilibrium (R_{eq}) at different ADAMTS13 concentrations), from different sets of proteins, were similar between *ADAMTS13* variants (Statistics: Mean ± SEM, One-way ANOVA).

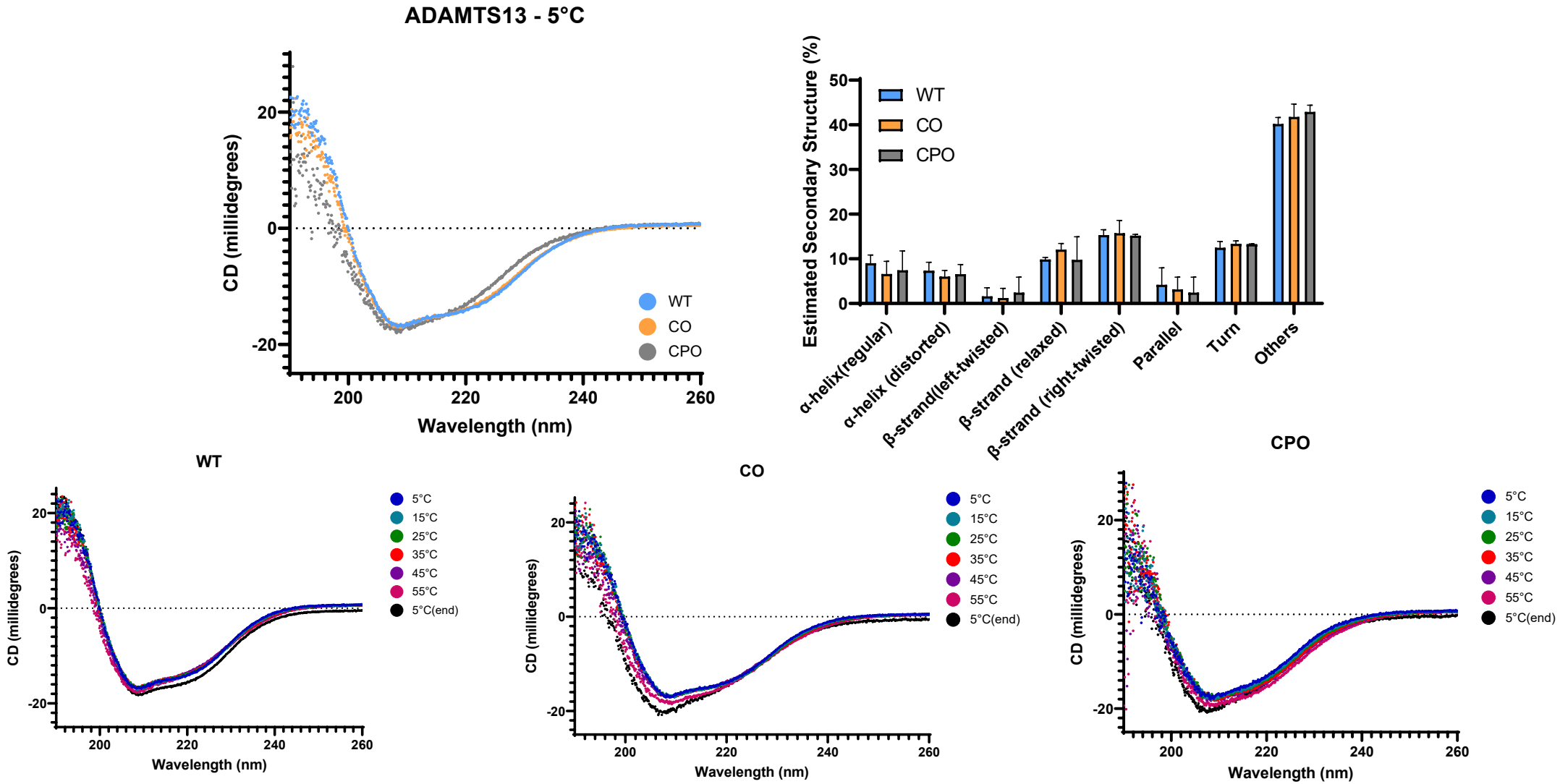

Supplementary Fig. 3: Circular Dichroism structure analysis of purified Flp-In derived WT, CO and CPO ADAMTS13 proteins for refolded structures. Structures were determined under unfolding (5°C→55°C) and refolding (55°C→5°C) temperature protocols at 10°C intervals. Initial graphs (above) represent initial 5°C and secondary structure estimation of CD (n = 3) using BestSel software for the initial spectra (Misconai et al., *Nucleic acids research* 2018), *no statistically significant differences in predicted secondary structure. Graphs below characterize the CD spectra of the ADAMTS13 variants throughout the unfolding process and then when refolded to 5°C. Noticeable differences were observed in refolding dynamics in CO and CPO variants.

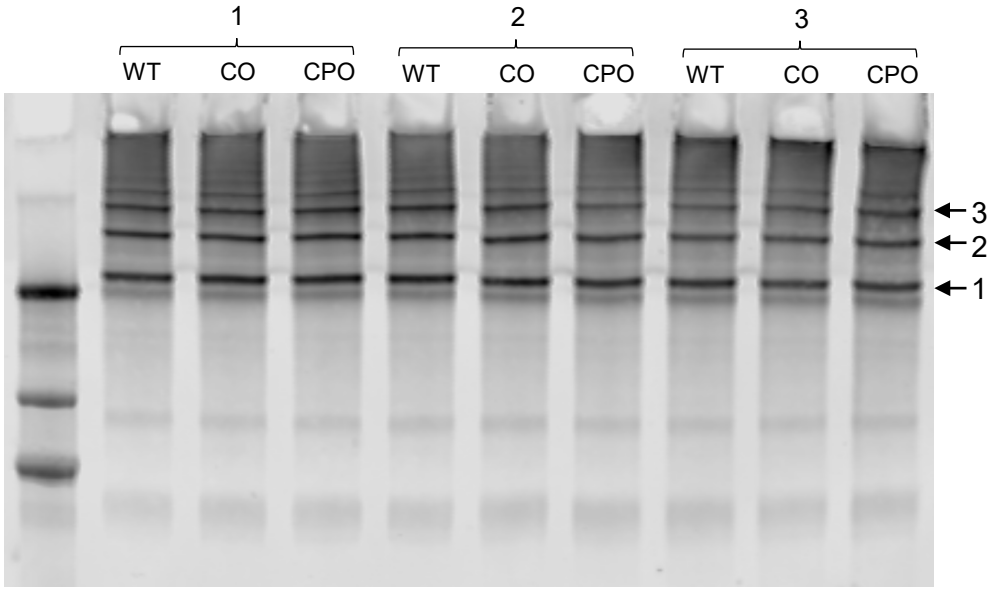

Supplementary Fig. 4: rVWF digestion with WT, CO and CPO ADAMTS13, derived from Flp-In cell lines showed similar activity. Assay was performed three times for 15 minutes at 2500 rpm, 37°C, under vortex conditions, showing one of three independent assays.

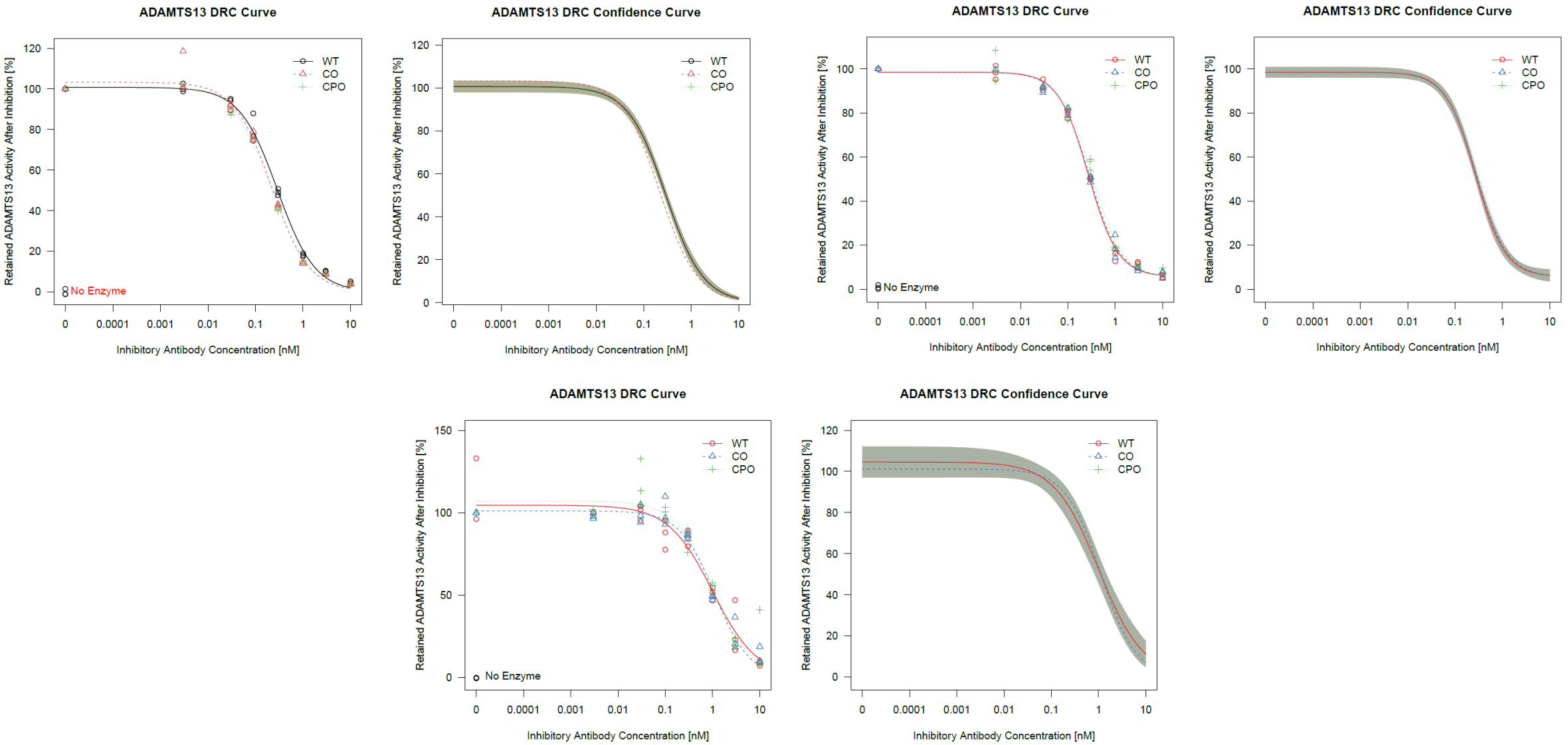

Supplementary Fig. 5: Inhibitory antibody assay with rADAMTS13 variant samples treated with monoclonal anti-ADAMTS13 antibody 3H9. Data from three batches showed similar inhibition kinetics for CO and CPO rADAMTS13 in comparison with wild type (WT) when incubated with the inhibitory antibody, with ED_{50} values 0.0311, 0.0257, and 0.0292 for WT; 0.0193, 0.0222, and 0.0244 for CO; 0.0227, 0.0221, and 0.0213 for CPO.

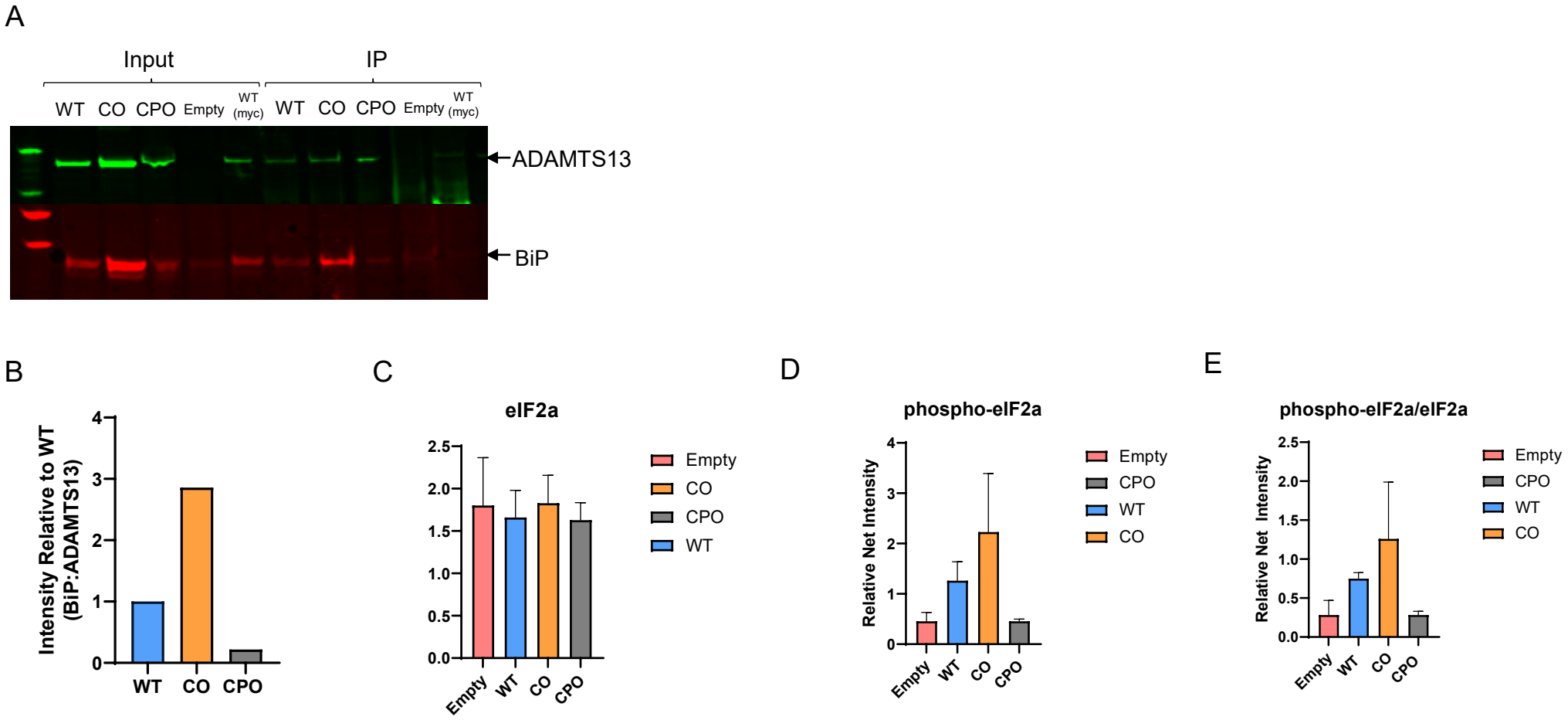

Supplementary Fig. 6: Altered bioenergetics and ER stress in *ADAMTS13* expressing cells. **(A)** Immunoprecipitation repeat experiment for assessing binding interaction between BiP and ADAMTS13. **(B)** Quantification of BiP immunoprecipitated in (A). **(C)** Flp-In derived lysates immunoblotted for eIF2a. **(D)** Flp-In derived lysates immunoblotted and probed for intracellular ER stress marker (p-eIF2α) expression. **(E)** quantification of ratio of phopho-eIF2a relative to eIF2a levels in Flp-In derived lysates as a measure of ER stress.

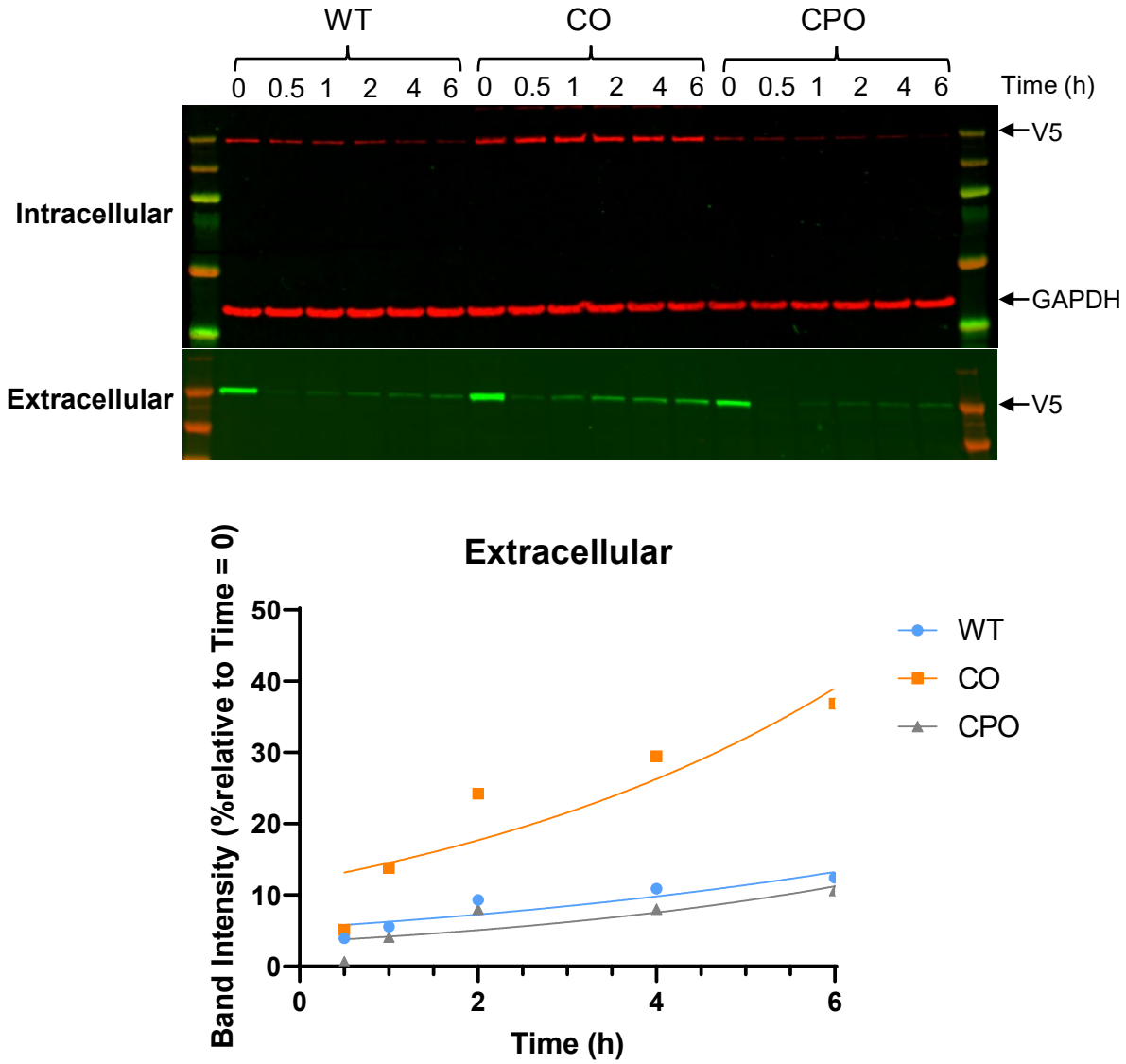

Supplementary Fig. 7: Relieving ER stress in CO *ADAMTS13*-expressing cells leads to increased secretion. Cycloheximide addition as an ER stress reliever leads to increased secretion of ADAMTS13 proteins.

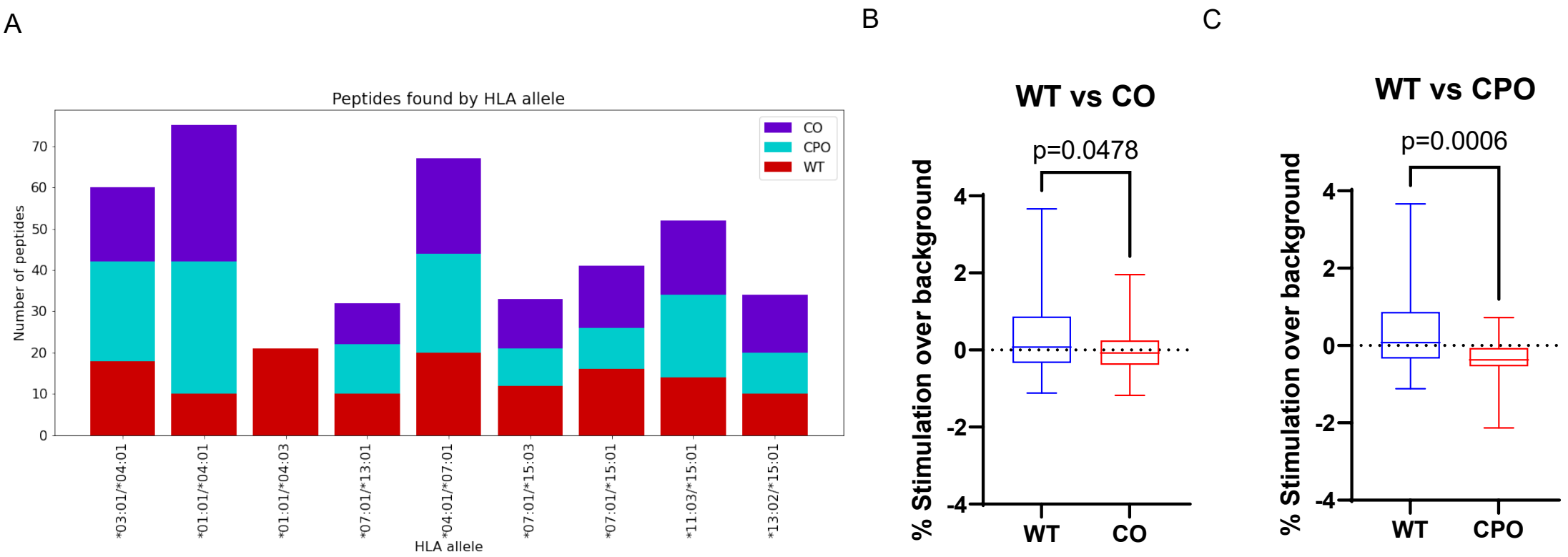

Supplementary Fig. 8: Altered immunogenicity profiles of CO and CPO ADAMTS13. (A) Differential presentation of WT, CO and CPO ADAMTS13-derived peptides bound to different MHC-II molecules was observed. (B) Immunogenicity profiles of WT vs CO and (C) WT vs CPO constructs based on a CD4+T-cell proliferation assay. Data are represented as %stimulation above background.

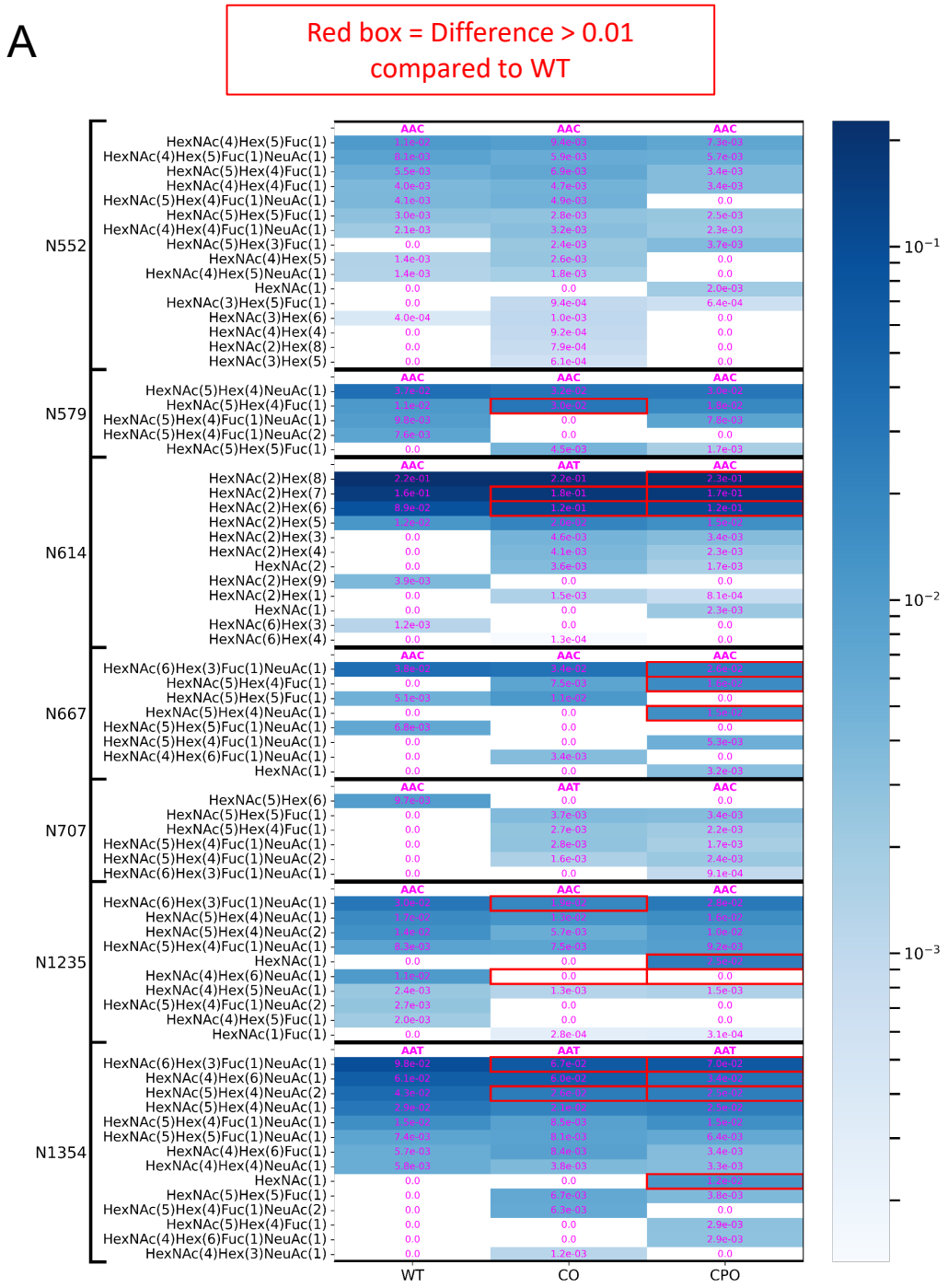

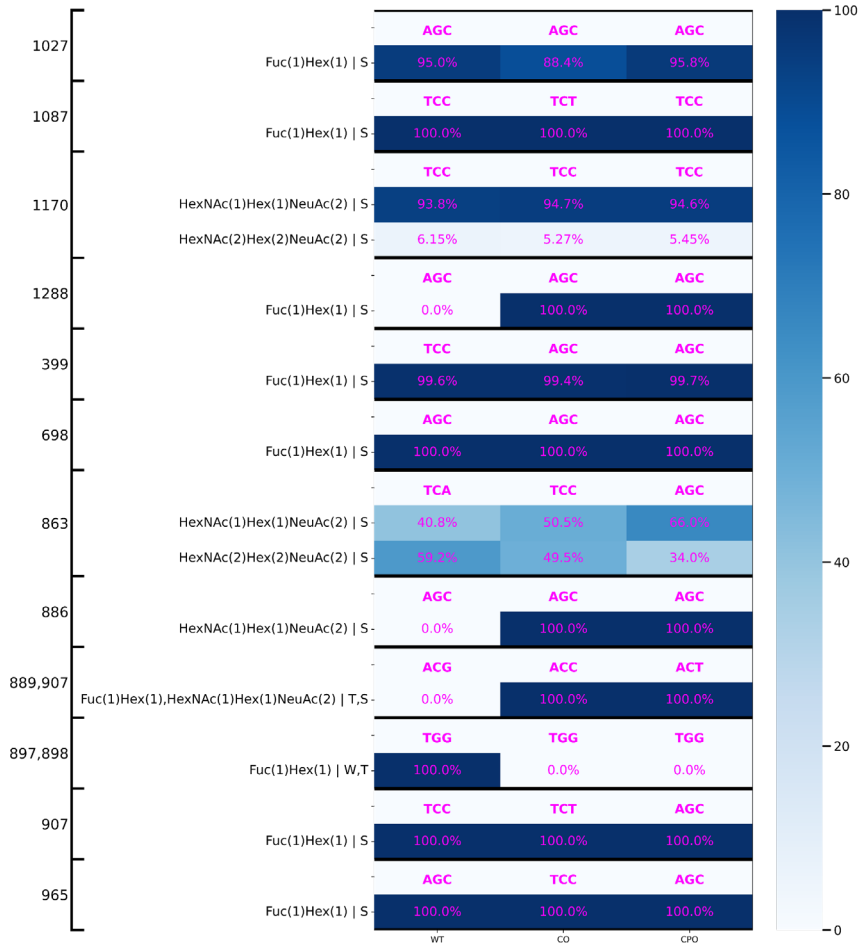

Supplementary Fig. 9 Post-translational modification analysis of purified Flp-In derived ADAMTS13 proteins. (A) Heatmap depicting abundance of all N-glycosylations at every site, as calculated by Byologic software. The codon identity at the site is labeled at the top of each block of the heatmap. The color bar is log-scaled. Red boxes highlight differences > 0.01 compared to WT. **(B)** Heatmap depicting the % ratio of O-fucosylation and C-mannosylation to the sum of WT and any other relevant modifications, as calculated by Byologic software sorted by codons that encode each amino acid modified at PTM sites.

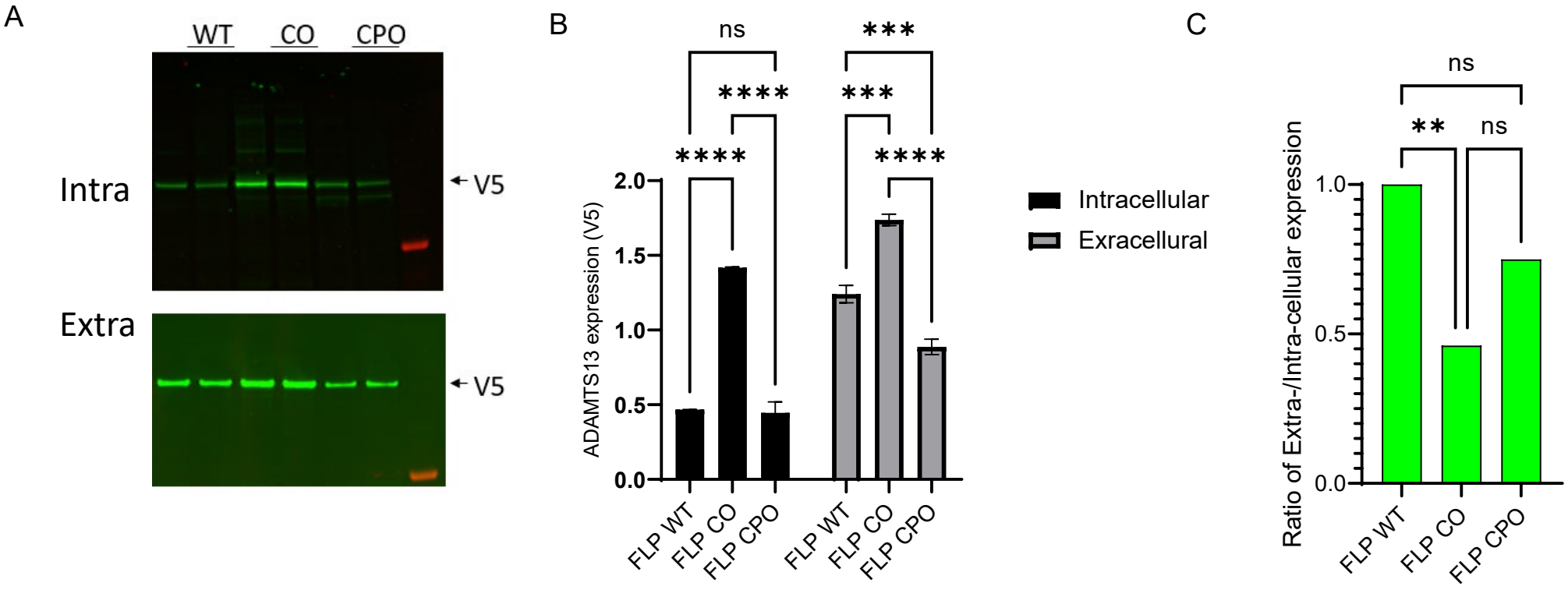

Supplementary Fig. 10: Synonymous Gene Recoding alter ADAMTS13 expression and secretion. (A) Immunoblot of intracellular and extracellular lysates of ADAMTS13 variants showing secretion of full-length and proteolyzed forms of ADAMTS13, probed with V5-tag antibody. **(B)** Quantification of blot shown in (A). **(C)** Ratio of Extra to Intra-cellular expression of ADAMTS13 in Flp-In cells to display the differenced in protein secretion (Statistics: Mean ± SEM, One-way ANOVA).

		Experiment 1			Experiment 2		
		WT	CO	CPO	WT	CO	CPO
Pos: 552	Codon	AAC	AAC	AAC	AAC	AAC	AAC
	HexNAc(4)Hex(5)Fuc(1)	1.050E-02	9.400E-03	7.290E-03	6.160E-03	1.960E-03	4.000E-03
	HexNAc(4)Hex(5)Fuc(1)NeuAc(1)	8.140E-03	5.930E-03	5.660E-03			
	HexNAc(5)Hex(4)Fuc(1)	5.460E-03	6.900E-03	3.420E-03	3.400E-03	2.570E-03	3.360E-03
Pos: 579	Codon	AAC	AAC	AAC	AAC	AAC	AAC
	HexNAc(5)Hex(4)NeuAc(1)	3.690E-02	3.150E-02	2.960E-02	1.090E-01	3.270E-02	1.820E-02
	HexNAc(5)Hex(4)Fuc(1)	1.080E-02	3.000E-02	1.840E-02	2.390E-02	9.740E-02	1.280E-01
	HexNAc(5)Hex(4)Fuc(1)NeuAc(1)	9.820E-03	0.000E+00	7.770E-03	2.870E-02	4.290E-02	3.680E-02
Pos: 614	Codon	AAC	AAT	AAC	AAC	AAT	AAC
	HexNAc(2)Hex(8)	2.170E-01	2.182E-01	2.270E-01	2.071E-01	1.622E-01	1.543E-01
	HexNAc(2)Hex(7)	1.592E-01	1.773E-01	1.737E-01	1.813E-01	1.737E-01	1.410E-01
	HexNAc(2)Hex(6)	8.918E-02	1.243E-01	1.162E-01	1.263E-01	1.591E-01	1.363E-01
Pos: 667	Codon	AAC	AAC	AAC	AAC	AAC	AAC
	HexNAc(6)Hex(3)Fuc(1)NeuAc(1)	3.810E-02	3.420E-02	2.640E-02	1.120E-02	5.540E-03	2.950E-02
	HexNAc(5)Hex(4)Fuc(1)	0.000E+00	7.470E-03	1.620E-02	0.000E+00	1.320E-02	3.030E-02
	HexNAc(5)Hex(5)Fuc(1)	5.140E-03	1.130E-02	0.000E+00	0.000E+00	5.480E-03	1.280E-02
Pos: 707	Codon	AAC	AAT	AAC	AAC	AAT	AAC
	HexNAc(5)Hex(6)	9.670E-03	0.000E+00	0.000E+00			
	HexNAc(5)Hex(5)Fuc(1)	0.000E+00	3.700E-03	3.420E-03	9.380E-03	7.790E-03	4.330E-03
	HexNAc(5)Hex(4)Fuc(1)	0.000E+00	2.670E-03	2.170E-03	5.780E-03	6.890E-03	7.480E-03
Pos: 1235	Codon	AAC	AAC	AAC	AAC	AAC	AAC
	HexNAc(6)Hex(3)Fuc(1)NeuAc(1)	3.040E-02	1.910E-02	2.810E-02	1.060E-02	1.460E-02	1.100E-02
	HexNAc(5)Hex(4)NeuAc(1)	1.690E-02	1.280E-02	1.560E-02	7.040E-03	7.100E-03	8.640E-03
	HexNAc(5)Hex(4)NeuAc(2)	1.400E-02	5.720E-03	1.010E-02			
Pos: 1354	Codon	AAT	AAT	AAT	AAT	AAT	AAT
	HexNAc(6)Hex(3)Fuc(1)NeuAc(1)	9.760E-02	6.710E-02	7.040E-02	3.530E-02	4.370E-02	3.490E-02
	HexNAc(4)Hex(6)NeuAc(1)	6.100E-02	6.030E-02	3.380E-02	1.550E-02	1.370E-02	1.480E-02
	HexNAc(5)Hex(4)NeuAc(2)	4.320E-02	2.620E-02	2.470E-02			

Supplementary Fig. 11. Comparison of PTM data from two separate experiments. A heatmap depicting the abundance of the top three N-glycosylations at each site, as calculated by Byologic software, identified in Experiment 1 (presented in this manuscript, Fig 2L, N and Supplementary Fig. 9), along with the levels of these glycans identified in Experiment 2. Due to slightly varying experimental designs, these cannot be treated as replicates for statistical analysis. The codon identity at each site is labeled at the top of each block in the heatmap. Experiment 1 shows the data presented in this manuscript, while Experiment 2 summarizes results from previous studies, where each variant was evaluated separately and therefore cannot be directly compared with others. Gray fields indicate glycans not detected.

Supplementary Tables

Supplementary Table 1. Predicted Translational Rate Differences (ADAMTS13 variants relative to WT).

Top 25th % CO-WT Differences		Top 25th % CPO-WT Differences		Bottom 25th % CO-WT Differences		Bottom 25th % CPO-WT Differences	
Overlapping Domain or Region	**Start-End (Difference)**	**Overlapping Domain or Region**	**Start-End (Difference)**	**Overlapping Domain or Region**	**Start-End (Difference)**	**Overlapping Domain or Region**	**Start-End (Difference)**
	51-75 (0.056)	TSP type-1 1	401-425 (0.043)	TSP type-1 3	751-775 (-0.016)	TSP type-1 4	826-850 (-0.015)
Disintegrin	351-375 (0.058)		1-25 (0.045)	TSP type-1 6	976-1000 (-0.016)	TSP type-1 5	901-925 (-0.021)
TSP type-1 8	1126-1150 (0.061)		51-75 (0.047)	Spacer	626-650 (-0.017)	CUB 2	1301-1325 (-0.022)
TSP type-1 5	876-900 (0.062)	Peptidase M12B,Disintegrin	276-300 (0.048)	CUB 2	1351-1375 (-0.02)	Spacer	651-675 (-0.023)
Peptidase M12B,Disintegrin	276-300 (0.066)		1151-1175 (0.05)	TSP type-1 3,TSP type-1 4	801-825 (-0.026)	Peptidase M12B	76-100 (-0.023)
TSP type-1 7,TSP type-1 8	1051-1075 (0.069)	Peptidase M12B	176-200 (0.051)	TSP type-1 1,Cysteine-rich	426-450 (-0.027)	CUB 1	1201-1225 (-0.029)
TSP type-1 1	401-425 (0.069)	TSP type-1 5	876-900 (0.051)	TSP type-1 3	776-800 (-0.028)	Disintegrin,TSP type-1 1	376-400 (-0.033)
TSP type-1 4	826-850 (0.071)	TSP type-1 6,TSP type-1 7	1001-1025 (0.054)	TSP type-1 2	701-725 (-0.031)	Cysteine-rich	451-475 (-0.033)
CUB 1,CUB 2	1276-1300 (0.081)	Cysteine-rich,Spacer	551-575 (0.056)	Peptidase M12B	226-250 (-0.042)	TSP type-1 1,Cysteine-rich	426-450 (-0.041)
Cysteine-rich,Spacer	551-575 (0.087)	Spacer	601-625 (0.061)	CUB 1	1251-1275 (-0.047)	CUB 1	1176-1200 (-0.044)
TSP type-1 5	926-950 (0.091)	TSP type-1 5	926-950 (0.062)	TSP type-1 2,Spacer	676-700 (-0.052)	Peptidase M12B	251-275 (-0.069)
Peptidase M12B	151-175 (0.094)	Peptidase M12B	126-150 (0.074)	Disintegrin	301-325 (-0.073)	TSP type-1 3	751-775 (-0.071)
CUB 2	1426-1450 (0.097)		26-50 (0.095)	Peptidase M12B	251-275 (-0.083)	Peptidase M12B	201-225 (-0.077)
Cysteine-rich	476-500 (0.099)	CUB 2	1426-1450 (0.097)	Disintegrin	326-350 (-0.084)	Disintegrin	301-325 (-0.086)
TSP type-1 4	851-875 (0.1)	TSP type-1 4	851-875 (0.1)	Cysteine-rich	451-475 (-0.087)	Peptidase M12B	226-250 (-0.096)

Supplementary Table 2. T-cell proliferation assay.
Table indicates that donors respond significantly to WT and CO ADAMTS13 proteins. None were significantly responsive to CPO.

Percent Stimulation above Background ≥0.5%, SEM=2			
Protein ID	**Responding Donor**	**% Stimulation**	**ANOVA (p value)**
ADAMTS13-WT	D29699	0.76	0.041
	D2771	0.86	0.026
	D2790	1.02	0.035
	D2791	0.72	0.018
	D3147	1.03	0.05
	D3148	2.27	0.037
ADAMTS13-CO	D2699	1.17	0.004
	D2767	0.54	0.022
	D2771	1.13	0.017

Supplementary Table 3. Post-translational modification analysis of purified Flp-In derived ADAMTS13 proteins. Most three abundant glycans in each glycosylation sites found in ADAMTS13 samples (WT, CO, CPO).

Position	Glycans	WT	CO	CPO
N552	HexNAc(4)Hex(5)Fuc(1)	**0.0105**	**0.0094**	**0.0073**
	HexNAc(4)Hex(5)Fuc(1)NeuAc(1)	0.0081	0.0059	0.0057
	HexNAc(5)Hex(4)Fuc(1)	0.0055	0.0069	0.0034
N579	HexNAc(5)Hex(4)NeuAc(1)	**0.0369**	**0.0315**	**0.0296**
	HexNAc(5)Hex(4)Fuc(1)	0.0108	0.0300	0.0184
	HexNAc(5)Hex(4)Fuc(1)NeuAc(1)	0.0098	0	0.0078
N614	HexNAc(2)Hex(8)	**0.2170**	**0.2182**	**0.2270**
	HexNAc(2)Hex(7)	0.1592	0.1773	0.1737
	HexNAc(2)Hex(6)	0.0892	0.1243	0.1162
N667	HexNAc(6)Hex(3)Fuc(1)NeuAc(1)	**0.0381**	**0.0342**	**0.0264**
	HexNAc(5)Hex(4)Fuc(1)	0	0.0075	0.0162
	HexNAc(5)Hex(5)Fuc(1)	0.0051	0.0113	0
N707	HexNAc(5)Hex(6)	**0.0097**	0	0
	HexNAc(5)Hex(5)Fuc(1)	0	**0.0037**	**0.0034**
	HexNAc(5)Hex(4)Fuc(1)	0	0.0027	0.0022
N1235	HexNAc(6)Hex(3)Fuc(1)NeuAc(1)	**0.0304**	**0.0191**	**0.0281**
	HexNAc(5)Hex(4)NeuAc(1)	0.0169	0.0128	0.0156
	HexNAc(5)Hex(4)NeuAc(2)	0.0140	0.0057	0.0101
N1354	HexNAc(6)Hex(3)Fuc(1)NeuAc(1)	**0.0976**	**0.0671**	**0.0704**
	HexNAc(4)Hex(6)NeuAc(1)	0.0610	0.0603	0.0338
	HexNAc(5)Hex(4)NeuAc(2)	0.0432	0.0262	0.0247

Supplementary Table 4. Post-translational modification analysis of purified Flp-In derived ADAMTS13 proteins. C-mannosylation and O-fucosylation sites found in all 3 samples, with % of modification (all modifications/peptide).

Positions	Modification Types	Glycopeptide Assignment of tryptic peptides*	Identified Sequence	% Modifications		
				WT	CO	CPO
262	W	Hex(1)	R.AGLAwSPCSR.R	100	100	0
387	W	Hex(1)	R.wSSWGPR.S	100	100	100
399	S	Fuc(1)Hex(1)	R.sCGGGVVTR.R	99.6	99.4	99.7
698	S	Fuc(1)Hex(1)	R.GPCSVsCGAGLR.W	100	100	100
863	S	HexNAc(1)Hex(1)NeuAc(2)	K.LPAPEPCVGMsCPPGWGHLDATSAGEK.A	40.8	50.5	66
		HexNAc(2)Hex(2)NeuAc(2)	K.LPAPEPCVGMsCPPGWGHLDATSAGEK.A	59.2	49.5	34
884	W	Hex(1)	K.APSPwGSIR.T	100	100	100
886	S	HexNAc(1)Hex(1)NeuAc(2)	K.APSPWGsIR.T	0	100	100
889,907	T,S	Fuc(1)Hex(1),HexNAc(1)Hex(1)NeuAc(2)	K.APSPWGSIRtGAQAAHVWTPAAGSCSVsCGR.G	0	100	100
897,898	W,T	Fuc(1)Hex(1)	R.TGAQAAHVwtPAAGSCSVSCGR.G	100	0	0
907	S	Fuc(1)Hex(1)	R.TGAQAAHVWTPAAGSCSVsCGR.G	100	100	100
965	S	Fuc(1)Hex(1)	K.LAACSVsCGR.G	100	100	100
1027	S	Fuc(1)Hex(1)	K.VMSLGPCSAsCGLGTAR.R	95	88.4	95.8
1087	S	Fuc(1)Hex(1)	R.WHVGTWMECSVsCGDGIQR.R	100	100	100
1170	S	HexNAc(1)Hex(1)NeuAc(2)	R.GLLFsPAPQPR.R	93.8	94.7	94.6
		HexNAc(2)Hex(2)NeuAc(2)	R.GLLFsPAPQPR.R	6.15	5.27	5.45
1288	S	Fuc(1)Hex(1)	R.CGRPGGGVLLRYGsQLAPETFYR.E	0	100	100

Supplementary Table 5. Glycan abundances for WT, CO, and CPO variants at each N-site based on heatmap in Fig. 8

Average Abundance per Site			
Position	WT	CO	CPO
1354	0.26509	0.2179	0.20277
1235	0.08733	0.046693	0.089438
707	0.00967	0.0107	0.010593
667	0.05007	0.05634	0.0661
614	0.48241	0.554054	0.541995
579	0.06508	0.06601	0.05751
552	0.040415	0.048923	0.030845

Supplementary Figures

A

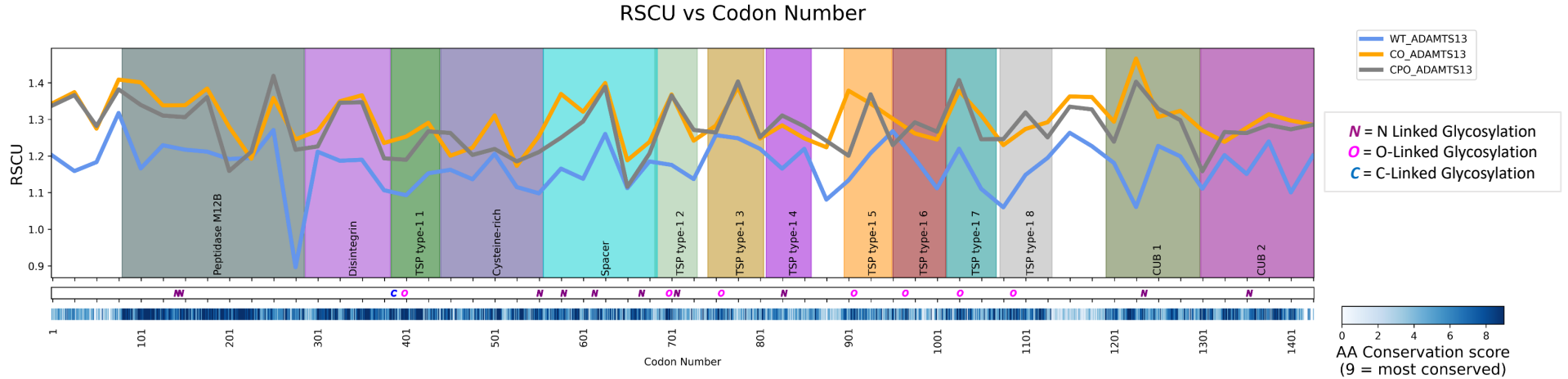
RSCU vs Codon Number
RSCU
Codon Number
Peptidase M12B
Disintegrin
TSP type-1 1
Cysteine-rich
Spacer
TSP type-1 2
TSP type-1 3
TSP type-1 4
TSP type-1 5
TSP type-1 6
TSP type-1 7
TSP type-1 8
CUB 1
CUB 2
WT_ADAMTS13
CO_ADAMTS13
CPO_ADAMTS13
N = N Linked Glycosylation
O = O-Linked Glycosylation
C = C-Linked Glycosylation
AA Conservation score
(9 = most conserved)

B

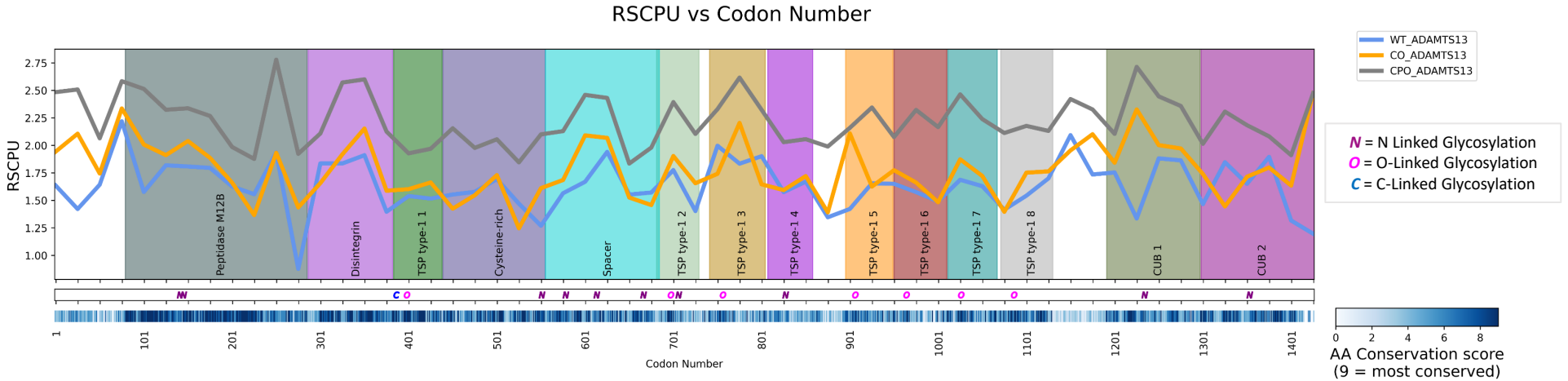
RSCPU vs Codon Number
RSCPU
Codon Number
Peptidase M12B
Disintegrin
TSP type-1 1
Cysteine-rich
Spacer
TSP type-1 2
TSP type-1 3
TSP type-1 4
TSP type-1 5
TSP type-1 6
TSP type-1 7
TSP type-1 8
CUB 1
CUB 2
WT_ADAMTS13
CO_ADAMTS13
CPO_ADAMTS13
N = N Linked Glycosylation
O = O-Linked Glycosylation
C = C-Linked Glycosylation
AA Conservation score
(9 = most conserved)

C

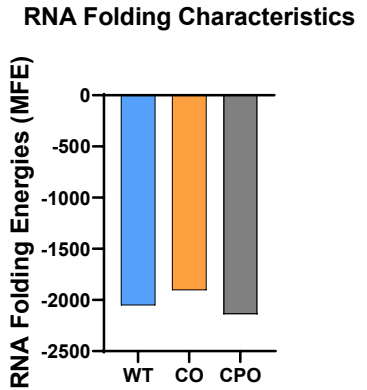
RNA Folding Characteristics
RNA Folding Energies (MFE)
WT
CO
CPO

D

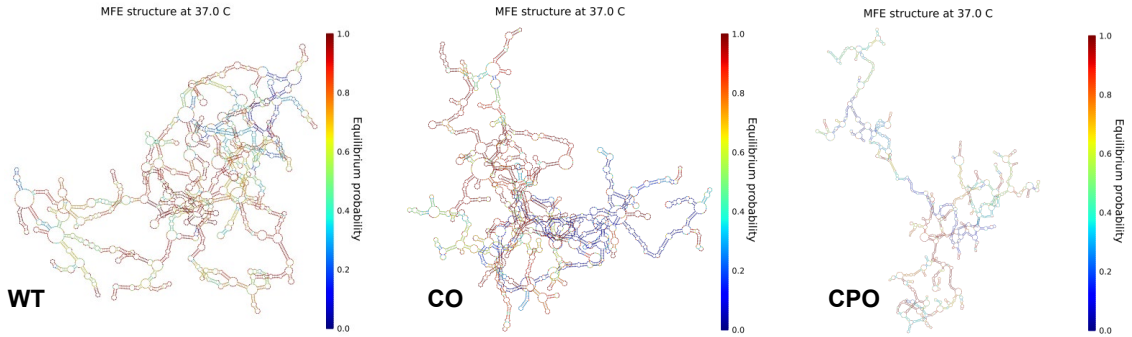
MFE structure at 37.0 C
Equilibrium probability
WT
CO
CPO

E

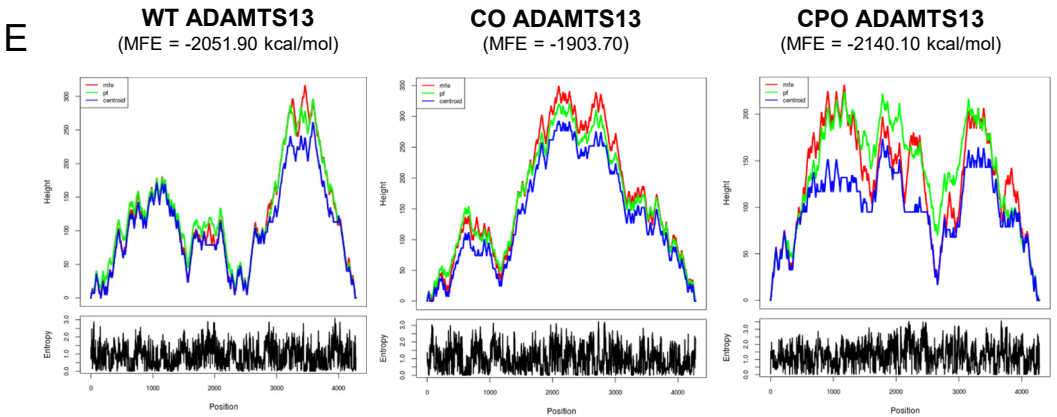
WT ADAMTS13
(MFE = -2051.90 kcal/mol)
CO ADAMTS13
(MFE = -1903.70)
CPO ADAMTS13
(MFE = -2140.10 kcal/mol)
Height
Entropy
Position

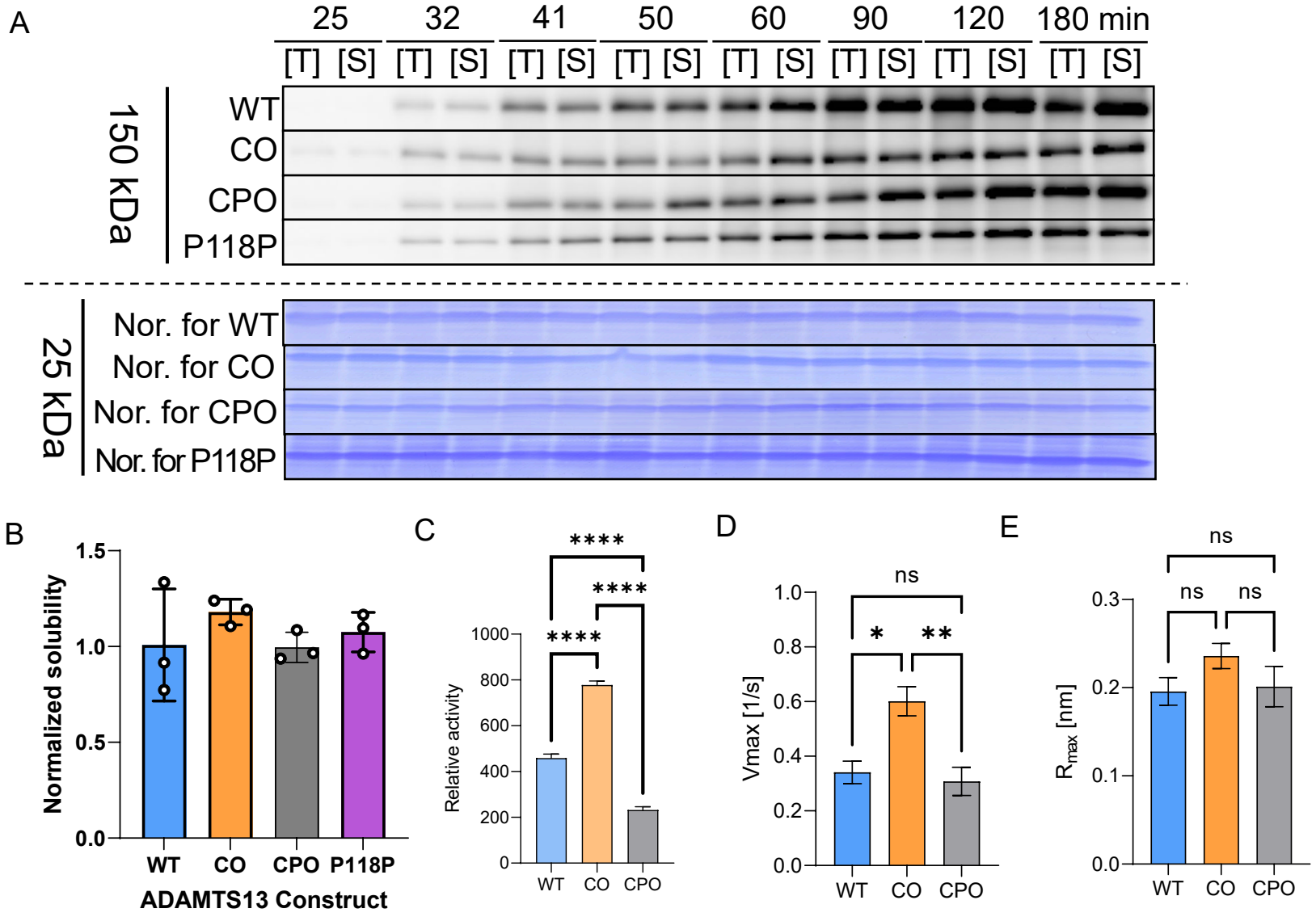

Supplementary Fig. 2: Kinetic analysis of ADAMTS13 variants. (A) Representative blotting of ADAMTS13 by RRL translation at multiple time points (upper panel) and the CBB staining for normalization (lower panel) used to calculate product concentration in Fig. 1C. **(B)** The solubility of ADAMTS13 from RRL assay at 180 min were similar between *ADAMTS13* variants (Statistically non-significant). **(C)** Activity of extracellular media, as measured by FRETS-VWF73 activity assay (dF/dt, [1/min]), used to calculate apparent specific activity in Fig. 1G, **(D)** FRETS activity assay with increasing VWF concentration and data was fitted with Michaelis Menten equation to derive kinetic values for Vmax, again showing significant changes in CO *ADAMTS13*. **(E)**, Maximum binding at equilibrium (R_{max}) determined from steady state analysis (nonlinear fitting of response at equilibrium (R_{eq}) at different ADAMTS13 concentrations), from different sets of proteins, were similar between *ADAMTS13* variants (Statistics: Mean ± SEM, One-way ANOVA).

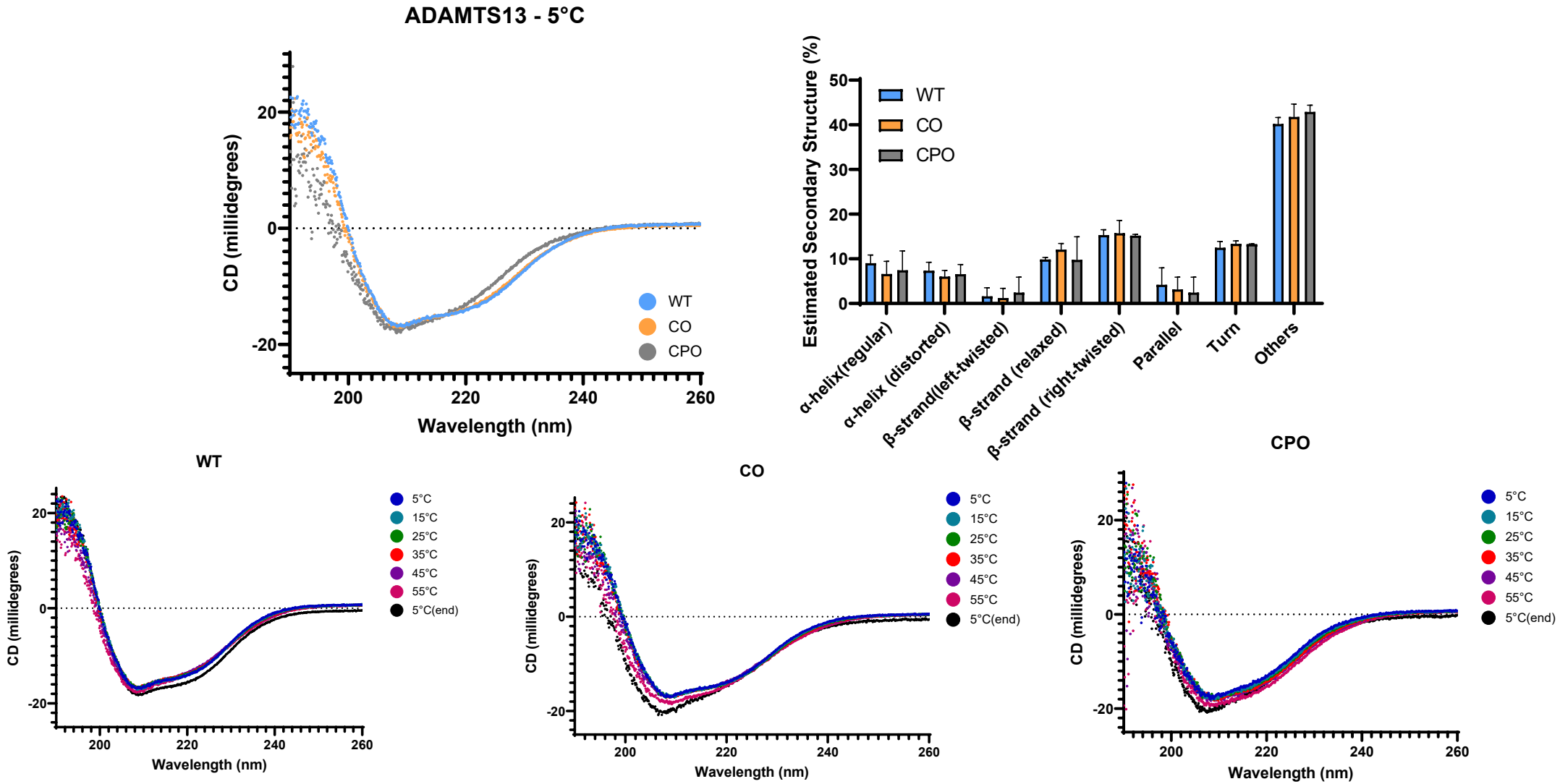

Supplementary Fig. 3: Circular Dichroism structure analysis of purified Flp-In derived WT, CO and CPO ADAMTS13 proteins for refolded structures. Structures were determined under unfolding (5°C→55°C) and refolding (55°C→5°C) temperature protocols at 10°C intervals. Initial graphs (above) represent initial 5°C and secondary structure estimation of CD (n = 3) using BestSel software for the initial spectra (Misconai et al., *Nucleic acids research* 2018), *no statistically significant differences in predicted secondary structure. Graphs below characterize the CD spectra of the ADAMTS13 variants throughout the unfolding process and then when refolded to 5°C. Noticeable differences were observed in refolding dynamics in CO and CPO variants.

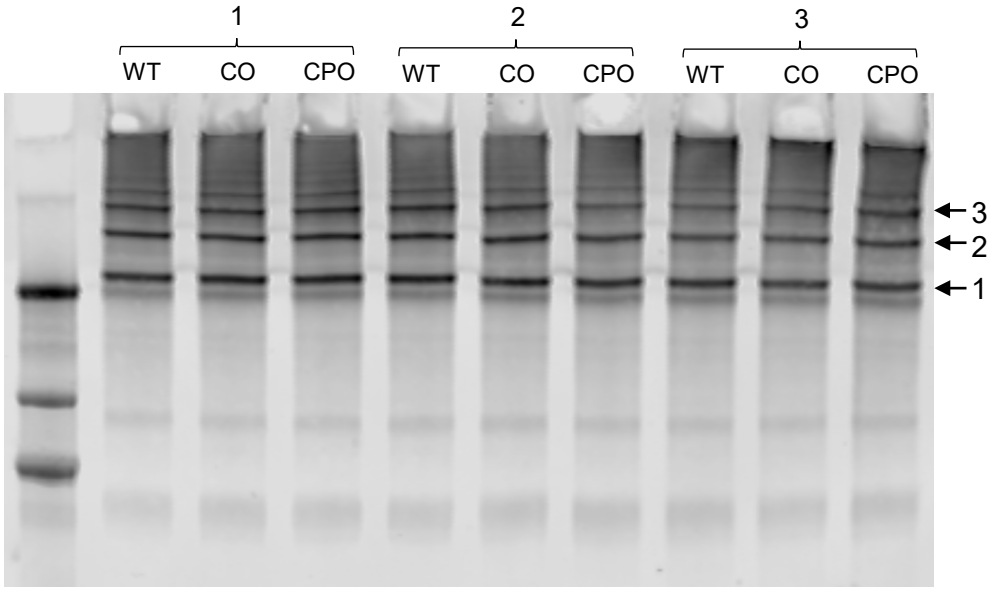

Supplementary Fig. 4: rVWF digestion with WT, CO and CPO ADAMTS13, derived from Flp-In cell lines showed similar activity. Assay was performed three times for 15 minutes at 2500 rpm, 37°C, under vortex conditions, showing one of three independent assays.

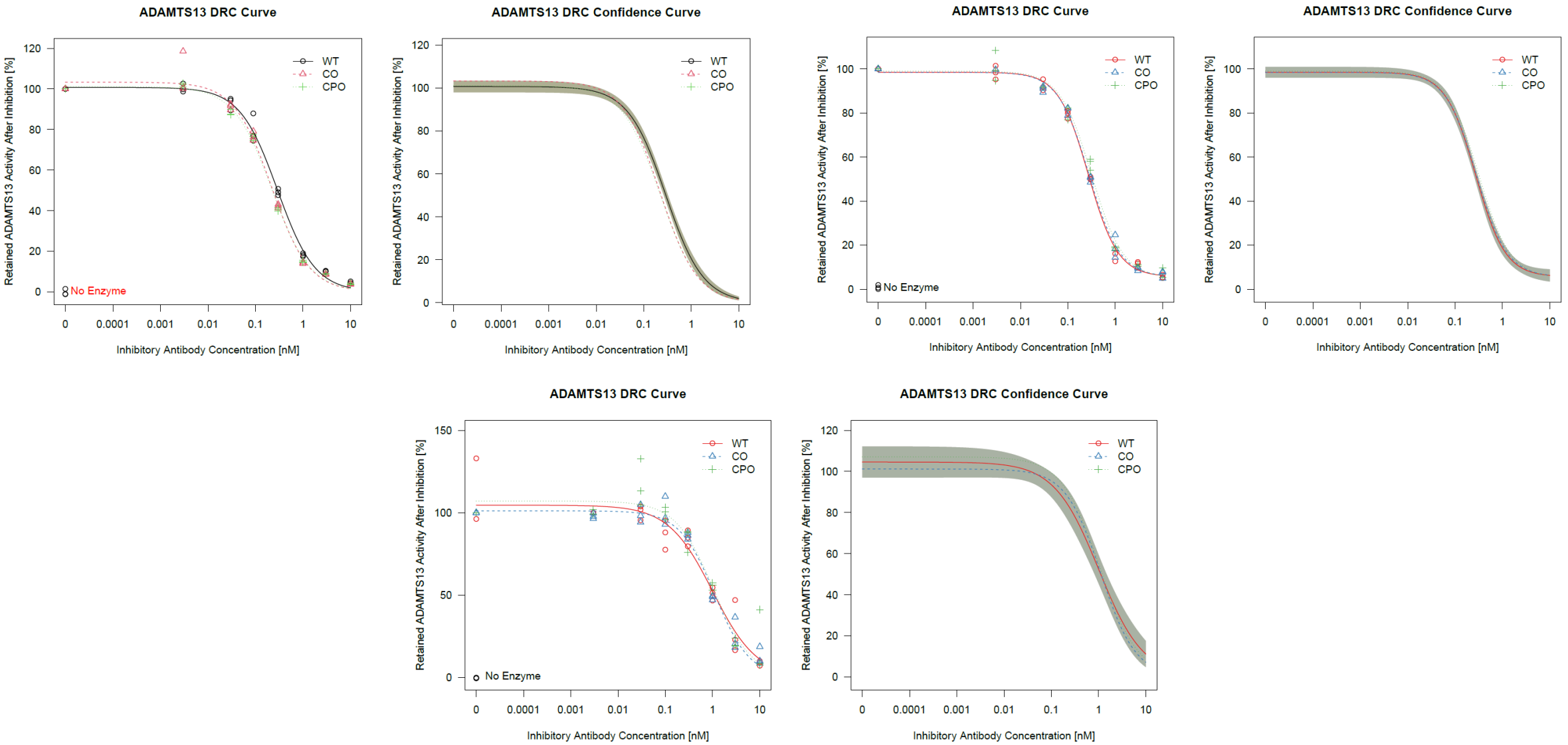

Supplementary Fig. 5: Inhibitory antibody assay with rADAMTS13 variant samples treated with monoclonal anti-ADAMTS13 antibody 3H9. Data from three batches showed similar inhibition kinetics for CO and CPO rADAMTS13 in comparison with wild type (WT) when incubated with the inhibitory antibody, with ED_{50} values 0.0311, 0.0257, and 0.0292 for WT; 0.0193, 0.0222, and 0.0244 for CO; 0.0227, 0.0221, and 0.0213 for CPO.

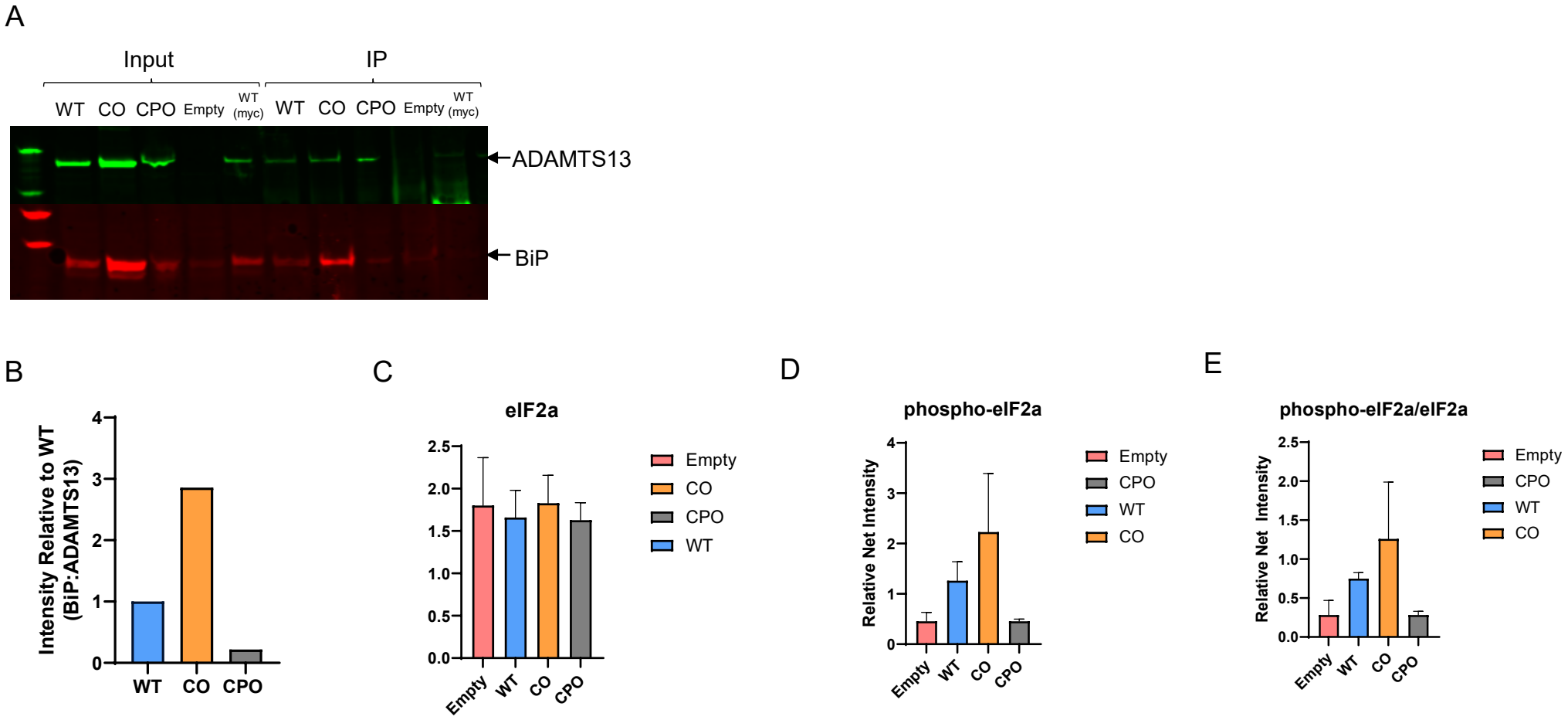

Supplementary Fig. 6: Altered bioenergetics and ER stress in *ADAMTS13* expressing cells. **(A)** Immunoprecipitation repeat experiment for assessing binding interaction between BiP and ADAMTS13. **(B)** Quantification of BiP immunoprecipitated in (A). **(C)** Flp-In derived lysates immunoblotted for eIF2a. **(D)** Flp-In derived lysates immunoblotted and probed for intracellular ER stress marker (p-eIF2α) expression. **(E)** quantification of ratio of phopho-eIF2a relative to eIF2a levels in Flp-In derived lysates as a measure of ER stress.

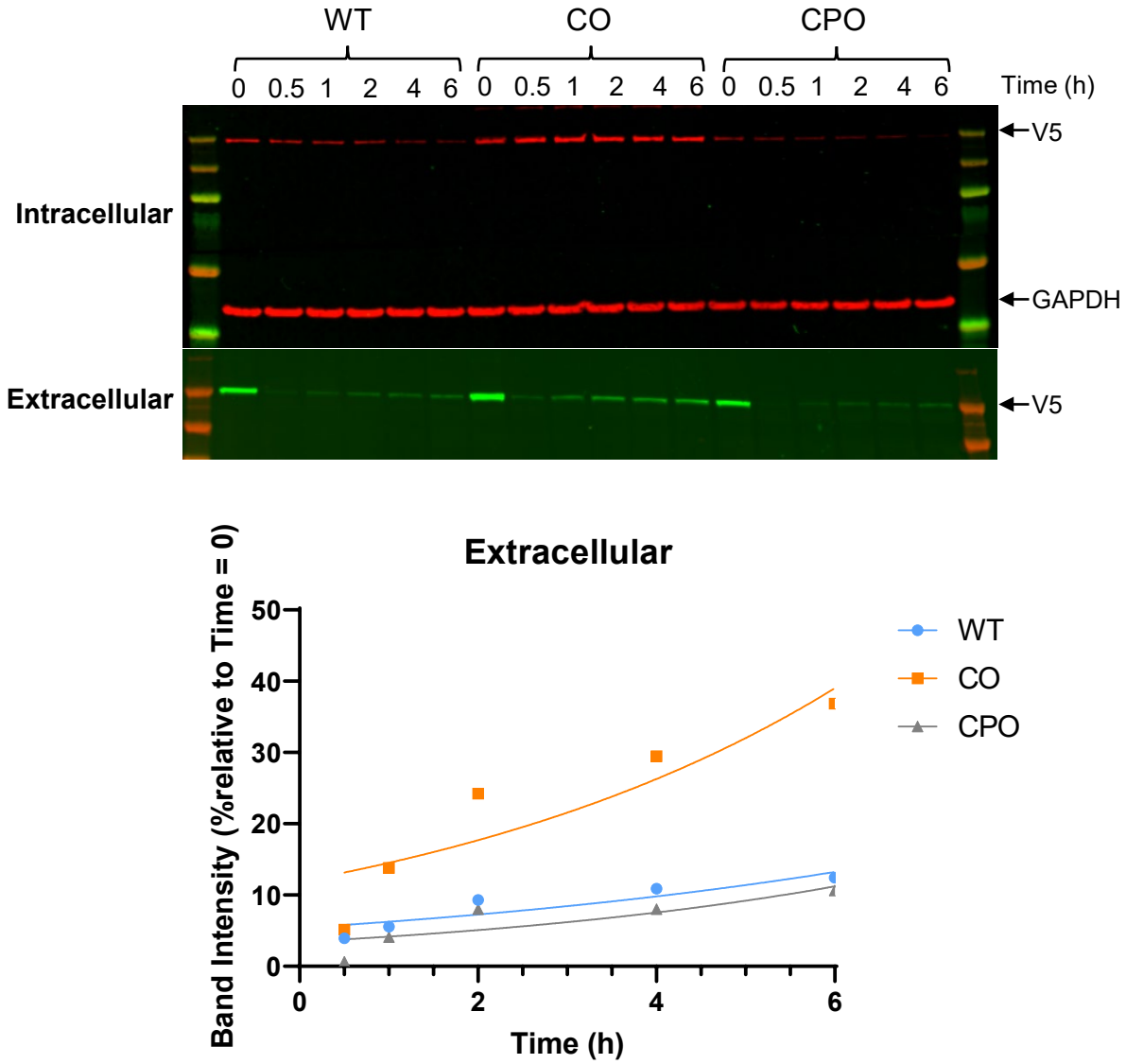

Supplementary Fig. 7: Relieving ER stress in CO *ADAMTS13*-expressing cells leads to increased secretion. Cycloheximide addition as an ER stress reliever leads to increased secretion of ADAMTS13 proteins.

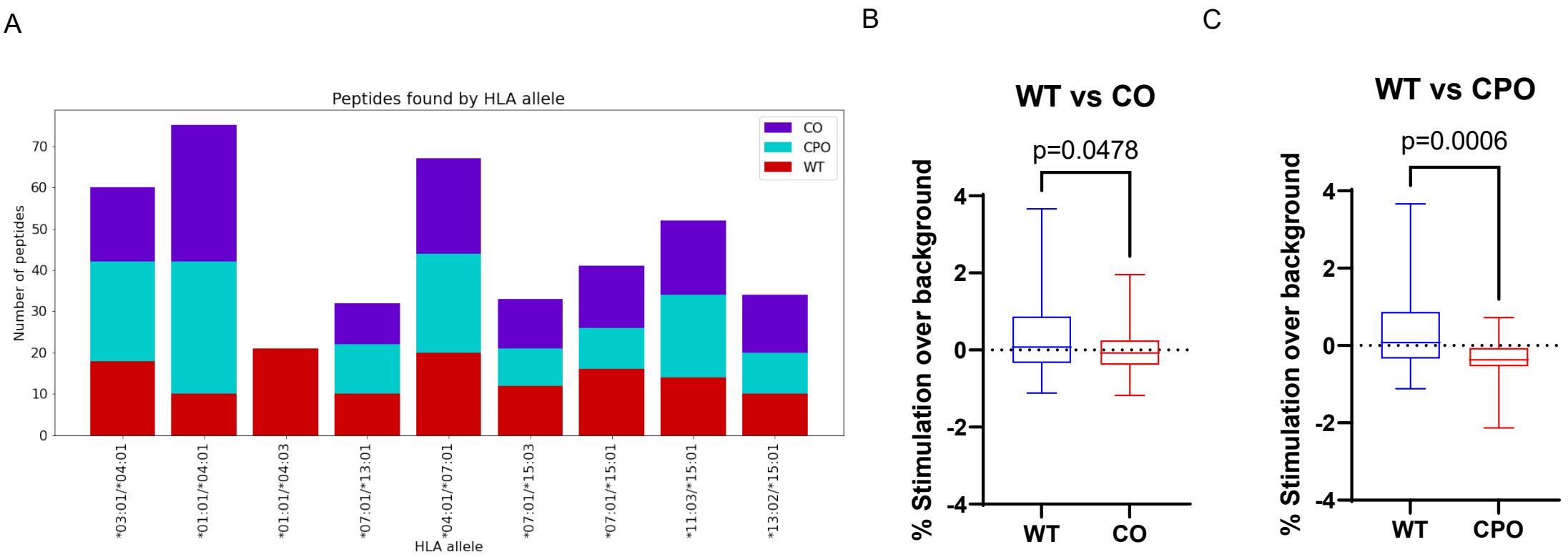

Supplementary Fig. 8: Altered immunogenicity profiles of CO and CPO ADAMTS13. (A) Differential presentation of WT, CO and CPO ADAMTS13-derived peptides bound to different MHC-II molecules was observed. (B) Immunogenicity profiles of WT vs CO and (C) WT vs CPO constructs based on a CD4+T-cell proliferation assay. Data are represented as %stimulation above background.

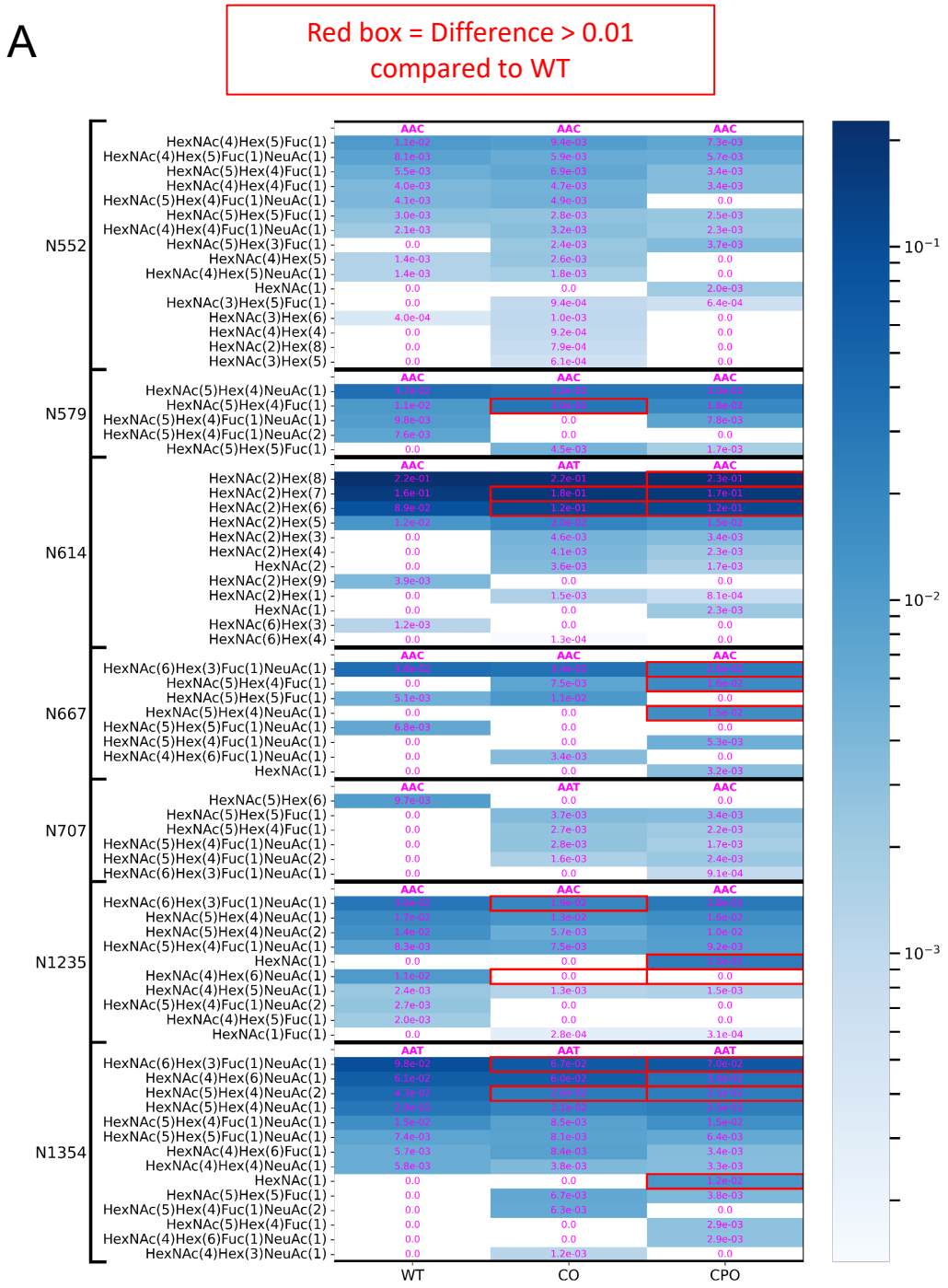

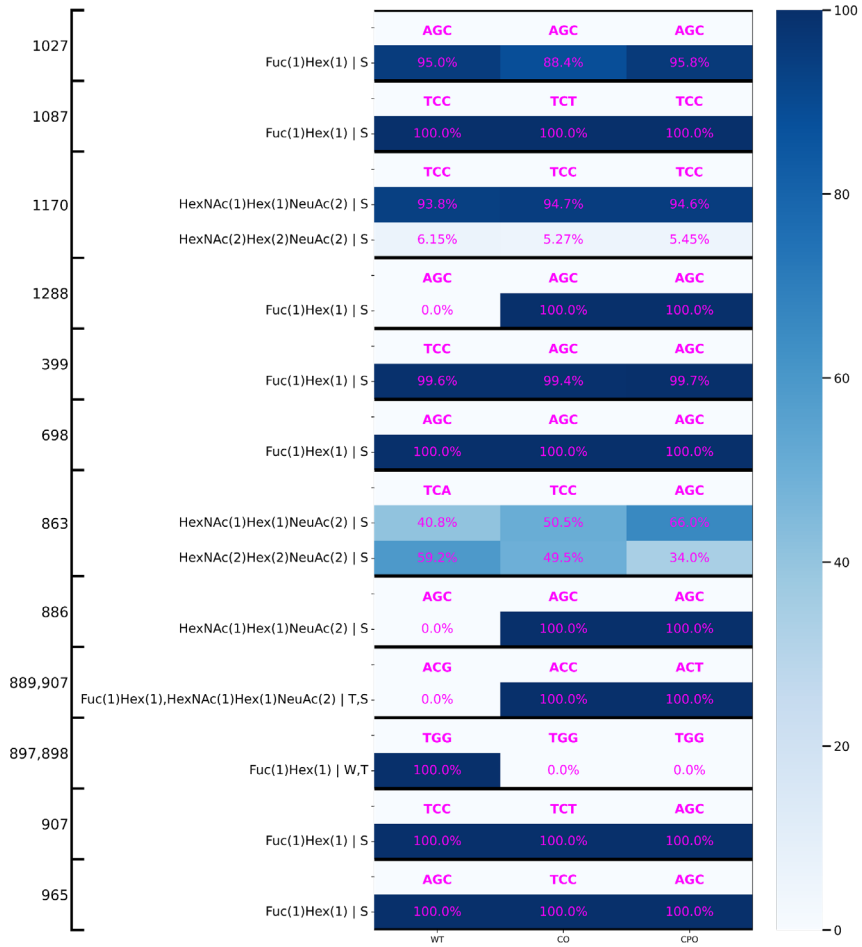

Supplementary Fig. 9 Post-translational modification analysis of purified Flp-In derived ADAMTS13 proteins. (A) Heatmap depicting abundance of all N-glycosylations at every site, as calculated by Byologic software. The codon identity at the site is labeled at the top of each block of the heatmap. The color bar is log-scaled. Red boxes highlight differences > 0.01 compared to WT. **(B)** Heatmap depicting the % ratio of O-fucosylation and C-mannosylation to the sum of WT and any other relevant modifications, as calculated by Byologic software sorted by codons that encode each amino acid modified at PTM sites.

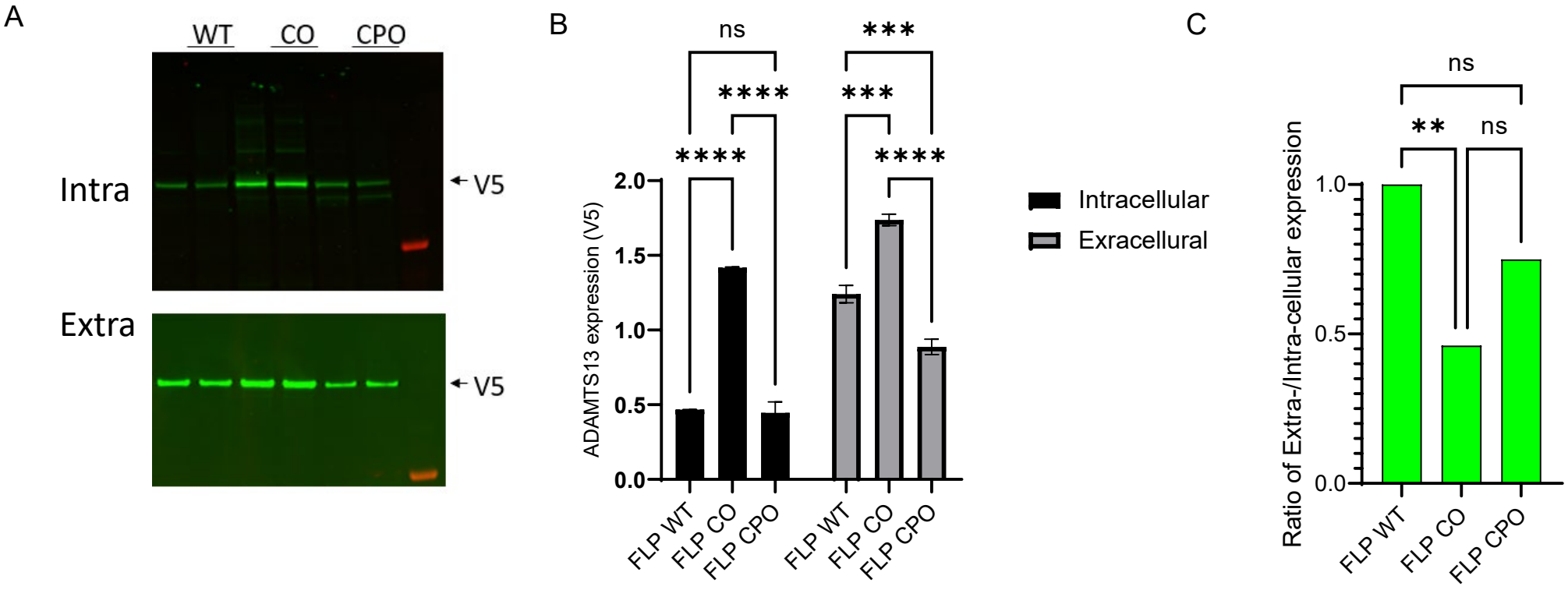

Supplementary Fig. 10: Synonymous Gene Recoding alter ADAMTS13 expression and secretion. (A) Immunoblot of intracellular and extracellular lysates of ADAMTS13 variants showing secretion of full-length and proteolyzed forms of ADAMTS13, probed with V5-tag antibody. **(B)** Quantification of blot shown in (A). **(C)** Ratio of Extra to Intra-cellular expression of ADAMTS13 in Flp-In cells to display the differenced in protein secretion (Statistics: Mean ± SEM, One-way ANOVA).

		Experiment 1			Experiment 2		
		WT	CO	CPO	WT	CO	CPO
Pos: 552	Codon	AAC	AAC	AAC	AAC	AAC	AAC
	HexNAc(4)Hex(5)Fuc(1)	1.050E-02	9.400E-03	7.290E-03	6.160E-03	1.960E-03	4.000E-03
	HexNAc(4)Hex(5)Fuc(1)NeuAc(1)	8.140E-03	5.930E-03	5.660E-03			
	HexNAc(5)Hex(4)Fuc(1)	5.460E-03	6.900E-03	3.420E-03	3.400E-03	2.570E-03	3.360E-03
Pos: 579	Codon	AAC	AAC	AAC	AAC	AAC	AAC
	HexNAc(5)Hex(4)NeuAc(1)	3.690E-02	3.150E-02	2.960E-02	1.090E-01	3.270E-02	1.820E-02
	HexNAc(5)Hex(4)Fuc(1)	1.080E-02	3.000E-02	1.840E-02	2.390E-02	9.740E-02	1.280E-01
	HexNAc(5)Hex(4)Fuc(1)NeuAc(1)	9.820E-03	0.000E+00	7.770E-03	2.870E-02	4.290E-02	3.680E-02
Pos: 614	Codon	AAC	AAT	AAC	AAC	AAT	AAC
	HexNAc(2)Hex(8)	2.170E-01	2.182E-01	2.270E-01	2.071E-01	1.622E-01	1.543E-01
	HexNAc(2)Hex(7)	1.592E-01	1.773E-01	1.737E-01	1.813E-01	1.737E-01	1.410E-01
	HexNAc(2)Hex(6)	8.918E-02	1.243E-01	1.162E-01	1.263E-01	1.591E-01	1.363E-01
Pos: 667	Codon	AAC	AAC	AAC	AAC	AAC	AAC
	HexNAc(6)Hex(3)Fuc(1)NeuAc(1)	3.810E-02	3.420E-02	2.640E-02	1.120E-02	5.540E-03	2.950E-02
	HexNAc(5)Hex(4)Fuc(1)	0.000E+00	7.470E-03	1.620E-02	0.000E+00	1.320E-02	3.030E-02
	HexNAc(5)Hex(5)Fuc(1)	5.140E-03	1.130E-02	0.000E+00	0.000E+00	5.480E-03	1.280E-02
Pos: 707	Codon	AAC	AAT	AAC	AAC	AAT	AAC
	HexNAc(5)Hex(6)	9.670E-03	0.000E+00	0.000E+00			
	HexNAc(5)Hex(5)Fuc(1)	0.000E+00	3.700E-03	3.420E-03	9.380E-03	7.790E-03	4.330E-03
	HexNAc(5)Hex(4)Fuc(1)	0.000E+00	2.670E-03	2.170E-03	5.780E-03	6.890E-03	7.480E-03
Pos: 1235	Codon	AAC	AAC	AAC	AAC	AAC	AAC
	HexNAc(6)Hex(3)Fuc(1)NeuAc(1)	3.040E-02	1.910E-02	2.810E-02	1.060E-02	1.460E-02	1.100E-02
	HexNAc(5)Hex(4)NeuAc(1)	1.690E-02	1.280E-02	1.560E-02	7.040E-03	7.100E-03	8.640E-03
	HexNAc(5)Hex(4)NeuAc(2)	1.400E-02	5.720E-03	1.010E-02			
Pos: 1354	Codon	AAT	AAT	AAT	AAT	AAT	AAT
	HexNAc(6)Hex(3)Fuc(1)NeuAc(1)	9.760E-02	6.710E-02	7.040E-02	3.530E-02	4.370E-02	3.490E-02
	HexNAc(4)Hex(6)NeuAc(1)	6.100E-02	6.030E-02	3.380E-02	1.550E-02	1.370E-02	1.480E-02
	HexNAc(5)Hex(4)NeuAc(2)	4.320E-02	2.620E-02	2.470E-02			

Supplementary Fig. 11. Comparison of PTM data from two separate experiments. A heatmap depicting the abundance of the top three N-glycosylations at each site, as calculated by Byologic software, identified in Experiment 1 (presented in this manuscript, Fig 2L, N and Supplementary Fig. 9), along with the levels of these glycans identified in Experiment 2. Due to slightly varying experimental designs, these cannot be treated as replicates for statistical analysis. The codon identity at each site is labeled at the top of each block in the heatmap. Experiment 1 shows the data presented in this manuscript, while Experiment 2 summarizes results from previous studies, where each variant was evaluated separately and therefore cannot be directly compared with others. Gray fields indicate glycans not detected.

Supplementary Tables

Supplementary Table 1. Predicted Translational Rate Differences (ADAMTS13 variants relative to WT).

Top 25th % CO-WT Differences		Top 25th % CPO-WT Differences		Bottom 25th % CO-WT Differences		Bottom 25th % CPO-WT Differences	
Overlapping Domain or Region	**Start-End (Difference)**	**Overlapping Domain or Region**	**Start-End (Difference)**	**Overlapping Domain or Region**	**Start-End (Difference)**	**Overlapping Domain or Region**	**Start-End (Difference)**
	51-75 (0.056)	TSP type-1 1	401-425 (0.043)	TSP type-1 3	751-775 (-0.016)	TSP type-1 4	826-850 (-0.015)
Disintegrin	351-375 (0.058)		1-25 (0.045)	TSP type-1 6	976-1000 (-0.016)	TSP type-1 5	901-925 (-0.021)
TSP type-1 8	1126-1150 (0.061)		51-75 (0.047)	Spacer	626-650 (-0.017)	CUB 2	1301-1325 (-0.022)
TSP type-1 5	876-900 (0.062)	Peptidase M12B,Disintegrin	276-300 (0.048)	CUB 2	1351-1375 (-0.02)	Spacer	651-675 (-0.023)
Peptidase M12B,Disintegrin	276-300 (0.066)		1151-1175 (0.05)	TSP type-1 3,TSP type-1 4	801-825 (-0.026)	Peptidase M12B	76-100 (-0.023)
TSP type-1 7,TSP type-1 8	1051-1075 (0.069)	Peptidase M12B	176-200 (0.051)	TSP type-1 1,Cysteine-rich	426-450 (-0.027)	CUB 1	1201-1225 (-0.029)
TSP type-1 1	401-425 (0.069)	TSP type-1 5	876-900 (0.051)	TSP type-1 3	776-800 (-0.028)	Disintegrin,TSP type-1 1	376-400 (-0.033)
TSP type-1 4	826-850 (0.071)	TSP type-1 6,TSP type-1 7	1001-1025 (0.054)	TSP type-1 2	701-725 (-0.031)	Cysteine-rich	451-475 (-0.033)
CUB 1,CUB 2	1276-1300 (0.081)	Cysteine-rich,Spacer	551-575 (0.056)	Peptidase M12B	226-250 (-0.042)	TSP type-1 1,Cysteine-rich	426-450 (-0.041)
Cysteine-rich,Spacer	551-575 (0.087)	Spacer	601-625 (0.061)	CUB 1	1251-1275 (-0.047)	CUB 1	1176-1200 (-0.044)
TSP type-1 5	926-950 (0.091)	TSP type-1 5	926-950 (0.062)	TSP type-1 2,Spacer	676-700 (-0.052)	Peptidase M12B	251-275 (-0.069)
Peptidase M12B	151-175 (0.094)	Peptidase M12B	126-150 (0.074)	Disintegrin	301-325 (-0.073)	TSP type-1 3	751-775 (-0.071)
CUB 2	1426-1450 (0.097)		26-50 (0.095)	Peptidase M12B	251-275 (-0.083)	Peptidase M12B	201-225 (-0.077)
Cysteine-rich	476-500 (0.099)	CUB 2	1426-1450 (0.097)	Disintegrin	326-350 (-0.084)	Disintegrin	301-325 (-0.086)
TSP type-1 4	851-875 (0.1)	TSP type-1 4	851-875 (0.1)	Cysteine-rich	451-475 (-0.087)	Peptidase M12B	226-250 (-0.096)

Supplementary Table 2. T-cell proliferation assay.
Table indicates that donors respond significantly to WT and CO ADAMTS13 proteins. None were significantly responsive to CPO.

Percent Stimulation above Background ≥0.5%, SEM=2			
Protein ID	**Responding Donor**	**% Stimulation**	**ANOVA (p value)**
ADAMTS13-WT	D29699	0.76	0.041
	D2771	0.86	0.026
	D2790	1.02	0.035
	D2791	0.72	0.018
	D3147	1.03	0.05
	D3148	2.27	0.037
ADAMTS13-CO	D2699	1.17	0.004
	D2767	0.54	0.022
	D2771	1.13	0.017

Supplementary Table 3. Post-translational modification analysis of purified Flp-In derived ADAMTS13 proteins. Most three abundant glycans in each glycosylation sites found in ADAMTS13 samples (WT, CO, CPO).

Position	Glycans	WT	CO	CPO
N552	HexNAc(4)Hex(5)Fuc(1)	**0.0105**	**0.0094**	**0.0073**
	HexNAc(4)Hex(5)Fuc(1)NeuAc(1)	0.0081	0.0059	0.0057
	HexNAc(5)Hex(4)Fuc(1)	0.0055	0.0069	0.0034
N579	HexNAc(5)Hex(4)NeuAc(1)	**0.0369**	**0.0315**	**0.0296**
	HexNAc(5)Hex(4)Fuc(1)	0.0108	0.0300	0.0184
	HexNAc(5)Hex(4)Fuc(1)NeuAc(1)	0.0098	0	0.0078
N614	HexNAc(2)Hex(8)	**0.2170**	**0.2182**	**0.2270**
	HexNAc(2)Hex(7)	0.1592	0.1773	0.1737
	HexNAc(2)Hex(6)	0.0892	0.1243	0.1162
N667	HexNAc(6)Hex(3)Fuc(1)NeuAc(1)	**0.0381**	**0.0342**	**0.0264**
	HexNAc(5)Hex(4)Fuc(1)	0	0.0075	0.0162
	HexNAc(5)Hex(5)Fuc(1)	0.0051	0.0113	0
N707	HexNAc(5)Hex(6)	**0.0097**	0	0
	HexNAc(5)Hex(5)Fuc(1)	0	**0.0037**	**0.0034**
	HexNAc(5)Hex(4)Fuc(1)	0	0.0027	0.0022
N1235	HexNAc(6)Hex(3)Fuc(1)NeuAc(1)	**0.0304**	**0.0191**	**0.0281**
	HexNAc(5)Hex(4)NeuAc(1)	0.0169	0.0128	0.0156
	HexNAc(5)Hex(4)NeuAc(2)	0.0140	0.0057	0.0101
N1354	HexNAc(6)Hex(3)Fuc(1)NeuAc(1)	**0.0976**	**0.0671**	**0.0704**
	HexNAc(4)Hex(6)NeuAc(1)	0.0610	0.0603	0.0338
	HexNAc(5)Hex(4)NeuAc(2)	0.0432	0.0262	0.0247

Supplementary Table 4. Post-translational modification analysis of purified Flp-In derived ADAMTS13 proteins. C-mannosylation and O-fucosylation sites found in all 3 samples, with % of modification (all modifications/peptide).

Positions	Modification Types	Glycopeptide Assignment of tryptic peptides*	Identified Sequence	% Modifications		
				WT	CO	CPO
262	W	Hex(1)	R.AGLAwSPCSR.R	100	100	0
387	W	Hex(1)	R.wSSWGPR.S	100	100	100
399	S	Fuc(1)Hex(1)	R.sCGGGVVTR.R	99.6	99.4	99.7
698	S	Fuc(1)Hex(1)	R.GPCSVsCGAGLR.W	100	100	100
863	S	HexNAc(1)Hex(1)NeuAc(2)	K.LPAPEPCVGMsCPPGWGHLDATSAGEK.A	40.8	50.5	66
		HexNAc(2)Hex(2)NeuAc(2)	K.LPAPEPCVGMsCPPGWGHLDATSAGEK.A	59.2	49.5	34
884	W	Hex(1)	K.APSPwGSIR.T	100	100	100
886	S	HexNAc(1)Hex(1)NeuAc(2)	K.APSPWGsIR.T	0	100	100
889,907	T,S	Fuc(1)Hex(1),HexNAc(1)Hex(1)NeuAc(2)	K.APSPWGSIRtGAQAAHVWTPAAGSCSVsCGR.G	0	100	100
897,898	W,T	Fuc(1)Hex(1)	R.TGAQAAHVwtPAAGSCSVSCGR.G	100	0	0
907	S	Fuc(1)Hex(1)	R.TGAQAAHVWTPAAGSCSVsCGR.G	100	100	100
965	S	Fuc(1)Hex(1)	K.LAACSVsCGR.G	100	100	100
1027	S	Fuc(1)Hex(1)	K.VMSLGPCSAsCGLGTAR.R	95	88.4	95.8
1087	S	Fuc(1)Hex(1)	R.WHVGTWMECSVsCGDGIQR.R	100	100	100
1170	S	HexNAc(1)Hex(1)NeuAc(2)	R.GLLFsPAPQPR.R	93.8	94.7	94.6
		HexNAc(2)Hex(2)NeuAc(2)	R.GLLFsPAPQPR.R	6.15	5.27	5.45
1288	S	Fuc(1)Hex(1)	R.CGRPGGGVLLRYGsQLAPETFYR.E	0	100	100

Supplementary Table 5. Glycan abundances for WT, CO, and CPO variants at each N-site based on heatmap in Fig. 8

Average Abundance per Site			
Position	WT	CO	CPO
1354	0.26509	0.2179	0.20277
1235	0.08733	0.046693	0.089438
707	0.00967	0.0107	0.010593
667	0.05007	0.05634	0.0661
614	0.48241	0.554054	0.541995
579	0.06508	0.06601	0.05751
552	0.040415	0.048923	0.030845